1-1-2019

Retro-foreland Basin Development in Response to Proto-Tethyan Ocean Closure, NE Tibet Plateau

Zhen Yan
Chinese Academy of Geological Sciences

Changlei Fu
Chinese Academy of Geological Sciences

Jonathan Aitchison

Solomon Buckman
University of Wollongong, solomon@uow.edu.au

Manlan Niu
Hefei University of Technology

See next page for additional authors

Retro-foreland Basin Development in Response to Proto-Tethyan Ocean Closure, NE Tibet Plateau

Abstract

2019. American Geophysical Union. All Rights Reserved. The compositions and ages of the sediments within retro or foreland basins that are formed and preserved adjacent to collisional orogens can reflect the nature of colliding tectonic elements. The nonmarine Yaoshuiquan and Huabaoshan formations in the South Qilian belt on the NE Tibetan Plateau deposited within a retro-foreland basin setting during latest Ordovician to Late Silurian time in response to arc-continent collision. Detritus derivation from a Cambro-Ordovician arc-ophiolite complex contains mixed 530-480 Ma oceanic-crust together with contributions from a 479-450 Ma continental-arc early in development of the basin. The Cambrian arc-accretionary system and Central Qilian block united to form the basement of a continental arc at ~450 Ma, and both then contributed sediments to the Lianhuashan-Huabaoshan basin. After the Hualong complex accreted to the north, a broad Andean-type margin developed along the southern margin of the Central Qilian block from 450 to 440 Ma. These processes generated a wider basin that received detritus from both the south and the north. Consumption of the Proto-Tethyan Ocean ended with collision between the Qaidam and Hualong blocks, which led to mass wasting of detritus from the Andean-type igneous rocks and both blocks with the basin from 440 to 420 Ma.

Publication Details

Yan, Z., Fu, C., Aitchison, J. C., Buckman, S., Niu, M., Cao, B., Sun, Y., Guo, X., Wang, Z. & Zhou, R. (2019). Retro-foreland Basin Development in Response to Proto-Tethyan Ocean Closure, NE Tibet Plateau. Tectonics, Online First 1-20.

Authors

Zhen Yan, Changlei Fu, Jonathan Aitchison, Solomon Buckman, Manlan Niu, Bo Cao, Yi Sun, Xianqing Guo, Zongqi Wang, and Renjie Zhou

Tectonics

RESEARCH ARTICLE
10.1029/2019TC005560

Special Section:
Collisional orogenic systems as recorders of collisions between arc and continents

Retro-foreland Basin Development in Response to Proto-Tethyan Ocean Closure, NE Tibet Plateau

Zhen Yan[1], Changlei Fu[1], Jonathan C. Aitchison[2], Solomon Buckman[3], Manlan Niu[4], Bo Cao[1], Yi Sun[4], Xianqing Guo[5], Zongqi Wang[5], and Renjie Zhou[2]

[1]Institute of Geology, Chinese Academy of Geological Sciences, Beijing, China, [2]School of Earth and Environmental Sciences, University of Queensland, Brisbane, Australia, [3]School of Earth and Environmental Sciences, University of Wollongong, Wollongong, Australia, [4]Department of Resources and Environment, Hefei University of Technology, Hefei, China, [5]Institute of Mineral Resources, Chinese Academy of Geological Sciences, Beijing, China

Abstract The compositions and ages of the sediments within retro or foreland basins that are formed and preserved adjacent to collisional orogens can reflect the nature of colliding tectonic elements. The nonmarine Yaoshuiquan and Huabaoshan formations in the South Qilian belt on the NE Tibetan Plateau deposited within a retro-foreland basin setting during latest Ordovician to Late Silurian time in response to arc-continent collision. Detritus derivation from a Cambro-Ordovician arc-ophiolite complex contains mixed 530-480 Ma oceanic-crust together with contributions from a 479-450 Ma continental-arc early in development of the basin. The Cambrian arc-accretionary system and Central Qilian block united to form the basement of a continental arc at ~450 Ma, and both then contributed sediments to the Lianhuashan-Huabaoshan basin. After the Hualong complex accreted to the north, a broad Andean-type margin developed along the southern margin of the Central Qilian block from 450 to 440 Ma. These processes generated a wider basin that received detritus from both the south and the north. Consumption of the Proto-Tethyan Ocean ended with collision between the Qaidam and Hualong blocks, which led to mass wasting of detritus from the Andean-type igneous rocks and both blocks with the basin from 440 to 420 Ma.

Key Points:
- The Yaoshuiquan and Huabaoshan formations of the Qilian Orogen record alluvial deposition in a retro-foreland basin
- The retro-foreland basin formed in response to collision of the Qaidam block and an Andean-type arc between 440 and 420 Ma
- Voluminous detritus shed from a Cambrian-age arc-ophiolite complex, micro-continental block, and Andean-type margin

Supporting Information:
- Supporting Information S1
- Data Set S1
- Data Set S2
- Data Set S3
- Data Set S4
- Data Set S5
- Data Set S6

Correspondence to:
Z. Yan,
yanzhen@mail.iggcas.ac.cn

Citation:
Yan, Z., Fu, C., Aitchison, J. C., Buckman, S., Niu, M., Cao, B., et al. (2019). Retro-foreland basin in the NE Tibet Plateau. *Tectonics*, *38*. https://doi.org/10.1029/2019TC005560

Received 3 MAY 2019
Accepted 7 OCT 2019
Accepted article online 19 OCT 2019

1. Introduction

Arc-continent collisions are an important tectonic process that drives growth of the continental crust and assembly of orogenic belts and flanking sedimentary basins throughout geological time (Aitchison et al., 2000; Aitchison & Buckman, 2012; Clift et al., 2003; Cooper & Taylor, 1987; Dewey, 2005). These collisions are observed today occurring along tectonically active plate boundaries such as those in the SW Pacific (e.g., Brown & Ryan, 2011). Numerous active collisional basins are forming near Papua New Guinea as result of collision between the Australian continent and the Banda Arc (Galewsky & Silver, 1997; Saqab et al., 2017) as well as near the island of Taiwan in response to collision of the Luzon volcanic arc with the eastern margin of continental Eurasia (Chen et al., 2001; Lundberg & Dorsey, 1988). These settings provide modern analogs for studies of crustal deformation and basin evolution in ancient collisional belts along former plate boundaries.

Ancient examples of plate collisions are commonly obscured or overprinted by later fragmentation and extensive reworking. They include Paleogene collision of a Tethyan intraoceanic island arc with the Indian continental margin prior to later continent-continent collision between India and Eurasia (e.g., Aitchison et al., 2000; Buckman et al., 2018; Corfield & Searle, 2000; Kapp & Decelles, 2019; Yin & Harrison, 2000); Ordovician arc-continent collision in the Irish Caledonides (Clift et al., 2009); and Ordovician collision of the intraoceanic Macquarie arc with the eastern margin of Gondwana in the Lachlan Fold Belt of eastern Australia (Aitchison & Buckman, 2012; Zhang et al., 2019). Collision-related sedimentary basins can become eroded and dismembered during and/or after the final stages of collision. Incomplete sedimentary records make it difficult to identify and understand the processes that might have occurred along associated plate boundaries. However, when preserved, their stratigraphy and deformation represent a valuable archive of the tectonic processes associated with the growth of continents through collision and suturing of island arcs, oceanic plateaus, and micro-continents onto continental margins.

China contains multiple orogens that developed as the Tarim, Qaidam, and North and South China blocks (Figure 1a) and numerous small micro-continental fragments that collided and coalesced throughout the Paleozoic to form a single aggregated continental landmass—Eurasia (Şengör & Natal'in, 1996; Sone & Metcalfe, 2008; Zuza et al., 2018). The Qilian Orogen in western China (Figure 1b) records closure of the Proto-Tethys Ocean through the Ordovician during which arc-continent preceded terminal continent-continent collision. Late Ordovician-Silurian sedimentary rocks are well-exposed in the Lajishan area along the northern margin of the South Qilian belt in the NE Tibet Plateau (Figure 1c). They were deposited in a retro-foreland basin located on and near the Lajishan suture between a Middle- to End-Ordovician continental arc and the Central Qilian block. This sedimentary sequence records the nature and timing of a multi-stage associated with the closure of the Proto-Tethyan Ocean along the northern margin of Tibet Plateau during the Early Paleozoic in which the effects of terminal continent-continent collision are superposed upon those of earlier arc-continent collision associated. Changes in sedimentary environments and detrital heavy mineral compositions record the collision and accretion of Tethys intraoceanic arc systems with micro-continental blocks during the Early Paleozoic. Although Mesozoic-Cenozoic deformation is active on the NE margin of the Tibetan Plateau (Zuza et al., 2018, and references therein), these intact sedimentary successions with well-developed sedimentary textures in the Lajishan area allow us to gain a better understanding of the nature of basin development and changes in depositional environments, provenance, and paleogeography during the process of arc-continent collision and eventual ocean closure.

In this paper, our goal is to provide details of the stratigraphic architecture and depositional environments of the Yaoshuiquan and Huabaoshan formations based on recent geological mapping. Petrographic and U-Pb age data of sandstones and conglomerate clasts provide a quantitative framework with which to consider closure of the Proto-Tethyan Ocean that occurred in response to arc-continental collision in the area that now constitutes the NE Tibet Plateau.

2. Geological Setting

The ~350 km wide, Qilian Orogen for ~1,200 km long trends NW-SE in the NE margin of the Tibetan Plateau (Figure 1a). It is the northernmost orogenic collage of the Tethyan domain and is surrounded by several micro-continent blocks such as North China, Tarim, and Qaidam. It formed in response to long-lived subduction and collision-related processes that led to formation of island arc, accretionary prism, ophiolite, seamount, high-pressure and ultrahigh-pressure (HP/UHP) metamorphic rocks, and associated sedimentary basins (e.g., Fu et al., 2018; Gehrels et al., 2003a, 2003b; Liu et al., 2018; Sobel & Arnaud, 1999; Wu et al., 2017; Xiao et al., 2009; Yan et al., 2010; Yan et al., 2019; Yin et al., 2007; Zhang et al., 2015). Ophiolites in the North and South Qilian belt have been interpreted as relics of two branches of the global Early Paleozoic ocean (Proto-Tethys Ocean) with seafloor spreading continuing to ca. 530 Ma (Xia et al., 2016; Song et al., 2017; Fu et al., 2018). These units were strongly modified by later phases of Mesozoic extension and Cenozoic intracontinental thrust and strike-slip faulting (Wu et al., 2016; Yin & Harrison, 2000; Zuza et al., 2018). Considerable attention had been paid to ophiolites and HP/UHP rocks, and several competing models for the tectonic evolution of this belt had been suggested. Considerable disagreement remains in respect of the temporal and spatial framework of the Qilian Orogen and details such as timing of subduction(s) and their associated polarities, early collision events, and final closure of oceanic basins. Much less consideration has been given to the sources and depositional setting of Paleozoic sedimentary rocks.

The Qilian Orogen is tectonically subdivisible from north to south into Northern, Central, and Southern Qilian belts (Figure 1b) on the basis of distinct lithostratigraphic units and geological structures. These belts were amalgamated by closure of the Proto-Tethyan Ocean during the Late Ordovician–Early Silurian (e.g., Song et al., 2013; Wu et al., 2016; Xia et al., 2003; Xiong & Coney, 1985; Zhang et al., 2015) or Devonian (e.g., Sobel & Arnaud, 1999; Smith et al., 2000; Gehrels et al., 2003a, 2003b; Xiao et al., 2009; Zuza et al., 2018).

The 1,200 × 100 km North Qilian belt is juxtaposed between the Alxa block to the North and the Central Qilian belt to the south. It is the most extensively studied element of the Qilian Orogen and contains elements of a Mariana-type intraoceanic subduction system including structurally dismembered elements of

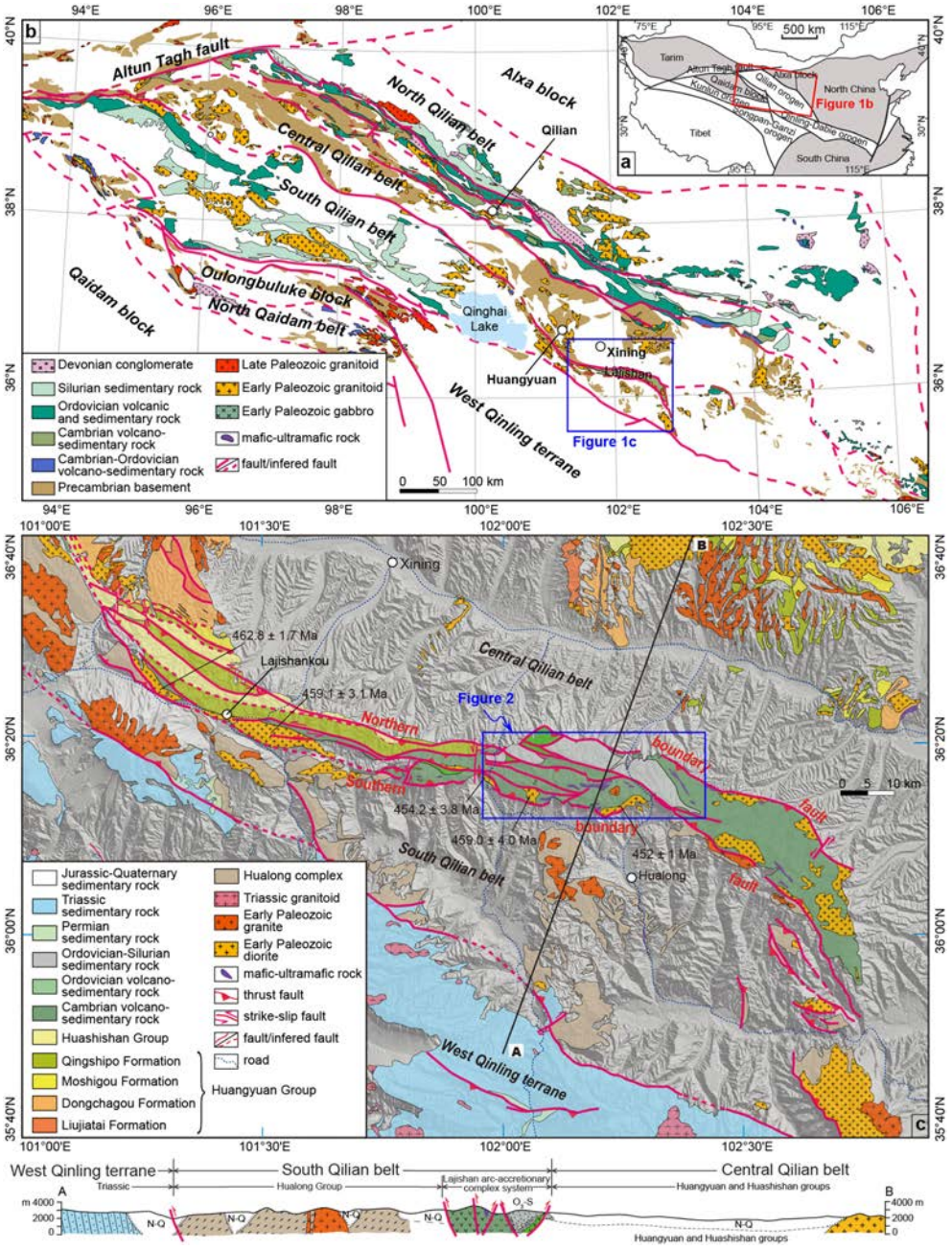

Figure 1. (a) Tectonic framework of China and location of the Qilian Orogen. (b) Geological map of the Qilian Orogen and location of the study area. (c) Geological map and cross section of the Lajishan and adjacent areas (modified after Yan et al., 2015; Fu et al., 2018) showing the relationship between different tectonic elements.

an accretionary complex, supra-subduction zone (SSZ)-ophiolite, island arc, and backarc/forearc basins (e.g., Song et al., 2013; Xia et al., 2003; Xiao et al., 2009; Yan et al., 2010).

The 1,000 by 80 km wide Central Qilian belt is separated from the North and South Qilian belts by SW-verging thrust faults. It is dominated by highly deformed, lower greenschist to amphibolite-facies Precambrian metamorphic rocks (Guo & Li, 1999; Liu et al., 2018; Tung et al., 2013; Wan et al., 2003) that have been intruded by Ordovician to Silurian I- and S-type granitoids (Tung et al., 2016). Rocks within a 240 x 80 km zone near Huangyuan County were originally assigned to the Neoproterozoic Huangyuan and Huashishan groups (BGMRQP, 1964). Together with the Neoproterozoic Hualong Complex in the

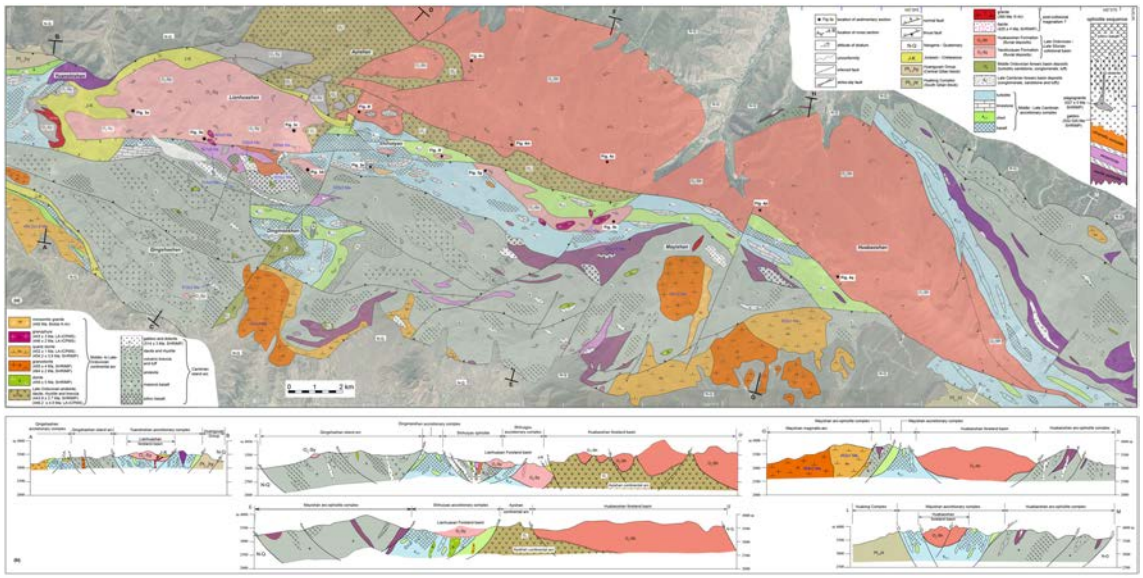

Figure 2. (a) Geological map of the central Lajishan area and inferred composite crustal column through Lajishan ophiolite complex based on our geological mapping results. (b) Cross sections and inferred interpretation of tectonic elements.

South Qilian belt, they have been interpreted as micro-continental blocks that separated from the South China plate during the late Neoproterozoic (Li et al., 2018; Tung et al., 2013; Yan et al., 2015).

Results of our recent geological mapping demonstrate that Early Paleozoic volcano-sedimentary strata in the Lajishan area include basalt, andesite, dacite, ultramafic rocks, gabbro, dolerite, chert, tuff, shale, turbiditic sandstone, and limestone (Figure 2a). The original stratigraphy is highly dismembered. Cambrian-age pillow and massive basalt with minor andesite, dacite, rhyolite, volcanic breccias, and volcaniclastic rocks in the Lajishan area represent products of an intraoceanic island arc (Fu et al., 2018; Fu & Yan, 2017). These rocks are structurally sandwiched between the Hualong complex to the south and Middle to Late Cambrian ophiolite-accretionary complex to the north. The accretionary complex consists of scaly black shale and siliceous mudstone matrix mélange that incorporates tectonic lenses of OIB- and MORB-basalt, red and green radiolarian chert, limestone, and turbiditic sandstone near Shihuiyao area. The complex extends eastward along northern margin of the Mayishan area and is juxtaposed against the Qingshashan-Mayishan arc-ophiolite complex to the south and Huabaoshan arc-ophiolite complex to the north. Together these units are in fault contact with the Neoproterozoic Hualong complex and Huangyuan Group in Yuanshishan and southern Mayishan areas (Figure 2b), respectively. Several intact volcano-sedimentary pillow basalt-limestone successions as well as laterally correlative basaltic breccia, interlayers of chert and tuff, thinner chert, and siliceous mudstone are well exposed around Shihuiyao, Dingmaoshan, and Mayishan areas. They exhibit lithologic successions similar to the famous Akiyoshi seamount within the accreted oceanic rocks in SW Japan (Sano & Kanmera, 1988). Abundant polymerid and agnostoid trilobites within limestone lenses (Lin et al., 2013; Lin et al., 2015) indicate that development of this oceanic plate stratigraphy continued in the Lajishan area until the Late Cambrian. Further west, a Middle to Late Cambrian (ca. 510-480 Ma) seamount sequence has been identified in the Lajishankou area (Figure 1b) on the basis of geological mapping together with petrological and geochemical data (Fu et al., 2014, 2018). These observations indicate that a south-facing intraoceanic subduction-accretion system developed during Cambrian time between the Central Qilian and the Hualong micro-blocks.

Regionally, in the Ayishan area, an intermediate to felsic composition volcano-sedimentary succession consisting of andesite, dacite, rhyolite, volcanic breccia, and volcaniclastic sandstone nonconformably overlies the Cambrian arc-accretionary complex system. These rocks were originally assigned to the Ayishan formation and attributed an Early Ordovician age (BGMRQP, 1964, 1991). However, our recent LA-ICP-MS zircon U-Pb studies yielded a terminal Ordovician weighted average $^{206}Pb/^{238}U$ age of 443.9 ± 2.7 Ma (MSWD = 2.7) and a Late Ordovician minimum peak age of 447 Ma for the rhyolite and rhyolitic tuff, respectively.

10.1029/2019TC005560

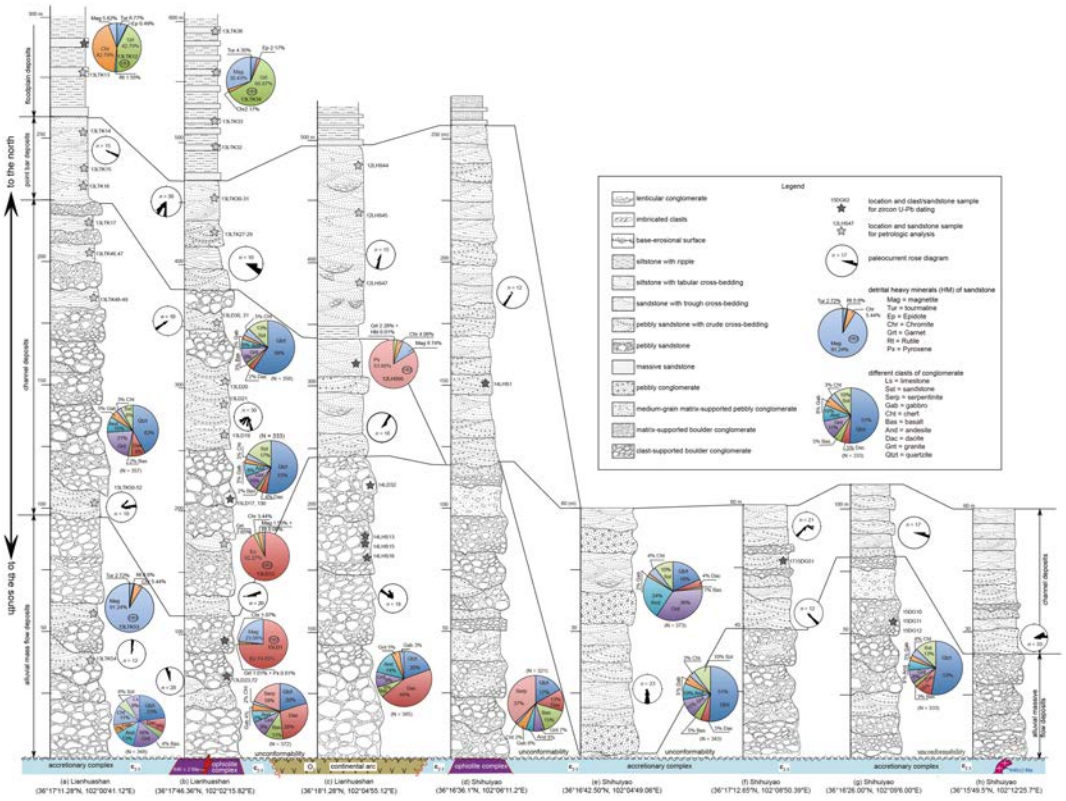

Figure 3. Measured sedimentary logs from the Yaoshuiquan Formation together with pie charts showing the relative abundance of clast types and detrital heavy minerals. Locations of logs are shown in Figure 2a.

Geochemical data demonstrate that the Ayishan volcanic rocks have typical subduction-related arc geochemical affinities. Voluminous Middle to Late Ordovician (464–446 Ma) subduction-related arc-type gabbro-diorite, diorite, quartz diorite, granophyre, and monzogranite intrusions crosscut the Cambrian arc-accretionary complex system. These intrusions represent the magmatic roots of a widespread Andean-type arc. LA-ICP-MS and SHRIMP zircon U-Pb ages demonstrate that granite and dacite dykes intruded into the Yaoshuiquan and Huabaoshan formations around the Shihuiyao area during the Silurian (443 ± 3 Ma and 420 ± 4 Ma, respectively). Recent work by Fu et al. (2018) on the ophiolite complex indicates that the Ayishan volcanic arc formed in response to northward subduction of the Proto-Tethyan Ocean following by a subduction flip, after the Cambrian arc-accretionary complex and the Central Qilian block collided.

Possible Late Ordovician to Early Silurian siliciclastic rocks (BGMRQP, 1964, 1976) nonconformably overlie both the Ayishan arc and Cambrian arc-accretionary system in the Lajishan area (Figure 2b). In turn they are covered by Mesozoic-Cenozoic sediments to the north. Until this study, no fossil and/or U-Pb data have been available from either formation. Zuo et al. (2001) suggested that these clastic rocks were deposited in an intramontane molasse basin, but Wang et al. (2016) recently suggested that they developed in a littoral environment associated with a forearc basin setting during Late Silurian to Early Devonian time. Our recent geological mapping results demonstrate that the Huabaoshan and Yaoshuiquan formations exhibit similar rock associations, sedimentary textures, and ages of formation.

Regionally, the Huabaoshan and Yaoshuiquan formations are mainly distributed across the north side of the Cambrian arc-ophiolite complex and accretionary complex. The Yaoshuiquan formation is separated from the Huabaoshan formation eastward by the Ayishan arc, respectively. The Yaoshuiquan formation also crops out in some discontinuous patches that nonconformably overlie the Cambrian oceanic arc and accretionary complex. The youngest detrital zircon peak ages of sandstones along with zircon U-Pb ages of crosscutting granitic plutons presented in this study demonstrate that both formations formed during the latest Ordovician to Late Silurian.

3. Sedimentary Facies and Depositional Environments

The thick alluvial successions of conglomerate, sandstone, and minor mudstone in the Huabaoshan and Yaoshuiquan formations fine northward. Our analysis is based on 14 measured sedimentary logs the locations of which are shown on Figure 2a.

3.1. Yaoshuiquan Formation

The 600 to 1200 m thick Yaoshuiquan formation comprises voluminous conglomerates and minor pebbly sandstone lenses, grading up-section into gray coarse-grained sandstone with minor lenticular conglomerates in the middle of the section and associations of sandstone and siltstone at higher levels. Fine-grained sediments of this formation are mainly exposed in the northern Lianhuashan area, and the abundance and thickness of conglomerate beds also decrease northward (Figure 3). Topographically, several discontinuous outcrops of the Yaoshuiquan formation that nonconformably overlie the Shihuiyao accretionary complex occur as isolated hills in which sedimentary successions <120 m thick are exposed. In addition, a 50 m wide conglomerate sequence of approximately 8 m thickness of the Yaoshuiquan formation overlies the Qingshashan Cambrian island-arc basalt and andesite assemblages.

The lower part of sections measured through the Yaoshuiquan formation contains thick, lenticular conglomerates and minor pebbly sandstone packages, with variable thicknesses between 20 and 230 m from east to west. Based on sandstone interlayers, conglomerate beds have an average thickness of 1.5–1.6 m. Conglomerates around the Shihuiyao arc-ophiolite and Yuanshishan accretionary complexes are mainly clast-supported and poorly organized (Figure 4a), but some conglomerate beds at higher levels exhibit distinct stratification (Figure 4b) due to variations of grain size and interbedded texture. Occasionally, clast- and matrix-supported conglomerates accompanied by thin sandstones are present as 3–4 m thick crude to well-developed fining-upward composite units. Clast size generally ranges from 3–25 cm in diameter and shows a distinct positive linear correlation with the thickness of conglomerate units. Clast imbrication, trough and tabular cross-beddings, and conspicuous irregular erosional base are common. These observations suggest deposition in a braided channel and bar sheet alluvial fan environment (Miall, 1985; Steel & Thompson, 1983).

The middle parts of the measured sections consist of conglomerate, coarse-grained sandstone, and sandstone with a thickness of circa 30–250 m. Conglomerates are mainly matrix-supported, crudely layered, poorly organized, and dominated by clasts 3–8 cm in diameter. They fine upward into pebbly sandstone. Sandstones show distinct planar cross-bedding with clast long axes parallel to foresets (Figure 4d). These rocks occur as stacked multi-story sheets with distinct erosion surfaces and a marked increase in grain size showing weakly developed coarse-tail grading and inverse grading locally. These characteristics are consistent with interpretation as alluvial sediments deposited from gravelly braided streams (Miall, 1985).

The upper parts of the measured sections consist of sandstone, siltstone, mudstone, and minor lenticular conglomerate, with a thickness of <700 m. Sandstones are mostly thick and commonly have conspicuous large-scale-scoured basal surfaces, and pebbly sandstones show distinct tabular and trough cross-bedding (Figure 4e). Siltstone contains abundant mica fragments and grades upward into mudstone with mudcracks. These rocks are interpreted to represent the products of floodplain environment that experienced subaerial exposures (Miall, 1985).

3.2. Huabaoshan Formation

The Huabaoshan formation consists of sandstone and minor conglomerate >3500 m thick (BGMRQP, 1964, 1976). Conglomerates are mainly exposed around the Ayishan arc and dramatically decrease in abundance eastward (Figure 5).

The lower parts of the measured sections consist of massive, matrix- and clast-supported conglomerate and minor sandstone, showing a fining-upward sequence. Conglomerates are poorly sorted and lack both internal bedding and clast imbrication (Figure 4f). However, these small-scale lenticular conglomerates within sandstones show dramatic basal erosion surfaces, clast imbrication (Figure 4g), and crude cross-bedding. A few, thin conglomerate units and only a few clasts thick commonly occur above basal erosion surfaces and exhibit fining-upward trends. Sandstones are highly lenticular with steep concave-up lower bounding surfaces and have abundant planar and trough cross-bedding with graded foresets and radical changes in

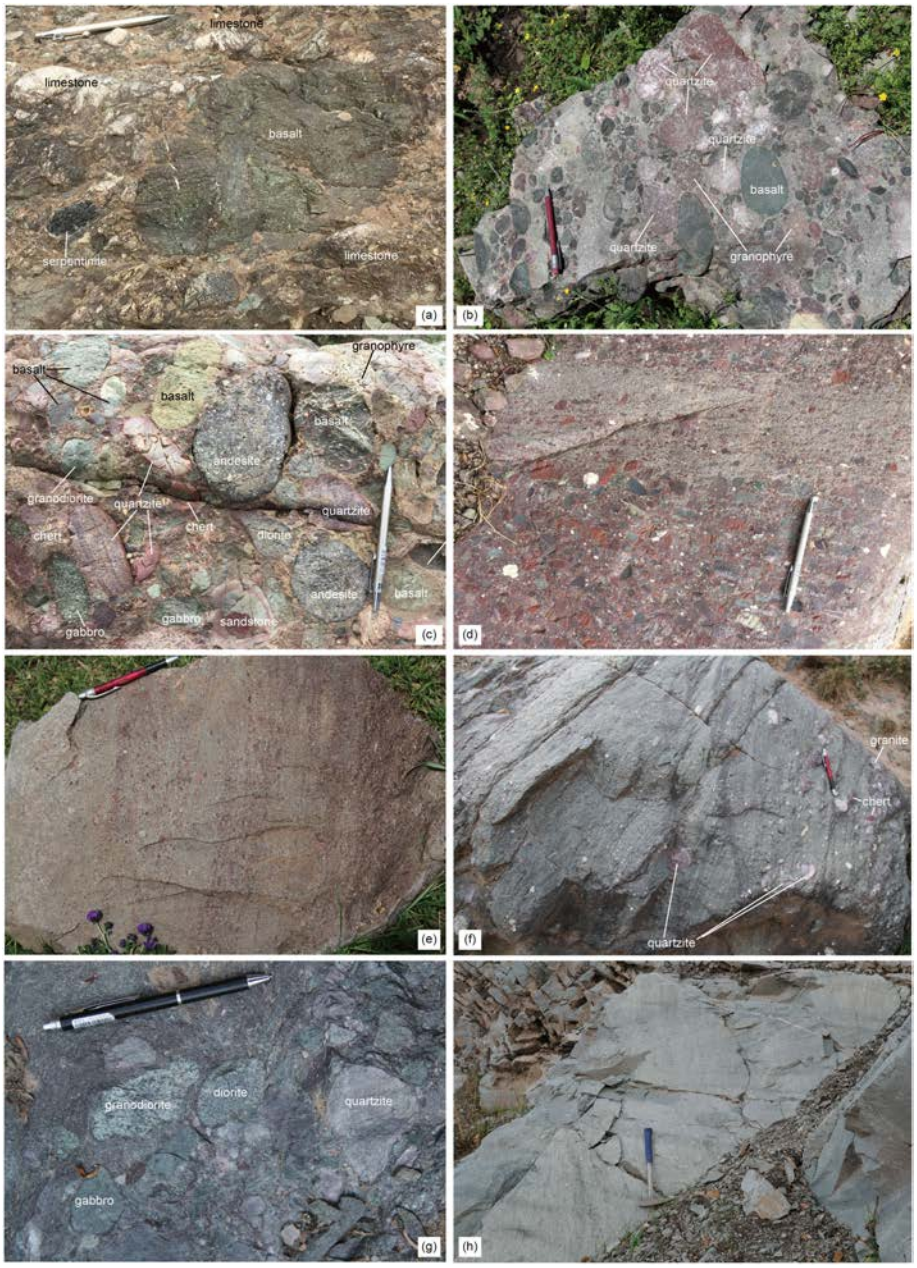

Figure 4. Typical outcrop photographs of the Yaoshuiquan (a to e) and Huabaoshan (f to h) formations. (a) Subangular and subrounded ophiolite-related clasts within conglomerate in the lower Lianhuashan section; (b) imbricated clasts in conglomerate at the middle Lianhuashan section; (c) coarse-grained conglomerate in the lower Lianhuashan section; (d) planar cross-bedding and imbricated clasts in pebbly sandstones and medium-grained conglomerates of the lower Lianhuashan section; and (e) trough cross-bedding in pebbly sandstone of the upper Lianhuashan section. (f) Trough and planar cross-bedding in pebbly sandstone of the lower Ayishan section. (g) Imbricated clasts in conglomerate of the lower Huabaoshan section; (h) planar cross-bedding in coarse-grained sandstone of the Huabaoshan section.

grain size along the set. These rocks are interpreted to represent point-bar deposits of a meandering channel and record a laterally migrating main channel and discharge fluctuations (Miall, 1985; Steel & Thompson, 1983).

The middle parts of the measured sections exhibit vertical upward-fining cyclical sequences of pebbly sandstone, sandstone, and minor siltstone, with a maximum thickness of >300 m. Coarse-grained sandstones are dramatically irregular and marked with scour and fill structures. Low-angle planar and trough cross-

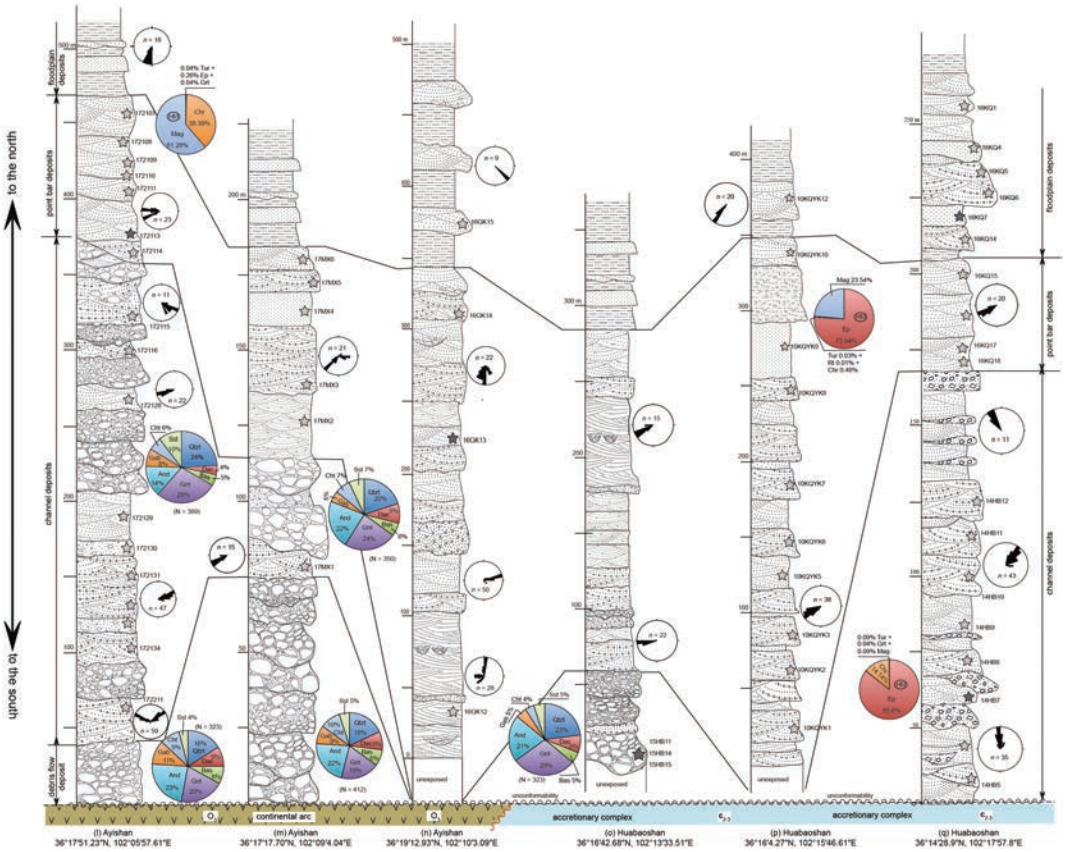

Figure 5. Measured sedimentary logs in the Huabaoshan formation together with pie charts showing the relative abundance of clast types and detrital heavy minerals. For locations of logs and details of the legend, see Figures 2a and 3.

bedding is common (Figure 4h); siltstones exhibit abundant small-scale ripple bedding and planar cross-bedding. These rocks are interpreted to represent braid bar deposits of a braided river system (Miall, 1985; Steel & Thompson, 1983).

The upper parts of the measured sections consist of gray siltstone and minor sandstone. Interlayers of siltstone and sandstone are <0.5 m thick and occur as lenticular wedges thinning over 10 s of meters. Sandstone is commonly massive and also has small-scale ripple bedding or trough cross-bedding with a low dip locally. Alternations of ripple-bedded sandstone and siltstone are the most frequent facies association. Minor 3–5 cm thick sandstones have conspicuous basal erosion surfaces and contain a few-rounded quartzite clast. These rocks are interpreted to represent products of an alluvial floodplain and small channels (Miall, 1985).

4. Sediment Composition

4.1. Conglomerates

In order to determine possible provenance, clast populations and abundance have been studied at 15 conglomerate outcrops in 10 measured sections according to the method of Dürr (1994). In each outcrop, about 320–420 pebbles, with diameters >5 cm, were measured. Clast lithologies include basalt, gabbro, andesite, dacite, granitoid, chert, limestone, sandstone, serpentinite, quartzite, gneiss, and schist. Individual clasts exhibit a dramatic range of sizes from 0.5 to 30 cm (long axis). They are angular to rounded in shape (Figure 4).

The abundance of quartzite and sandstone clasts increases up-section (Figures 3 & 5), whereas the abundance of basalt, gabbro, chert, limestone, and serpentinite clasts decreases. Spatially, the abundance of quartzite and sandstone clasts dramatically increases from south to north, whereas that of ophiolitic clasts

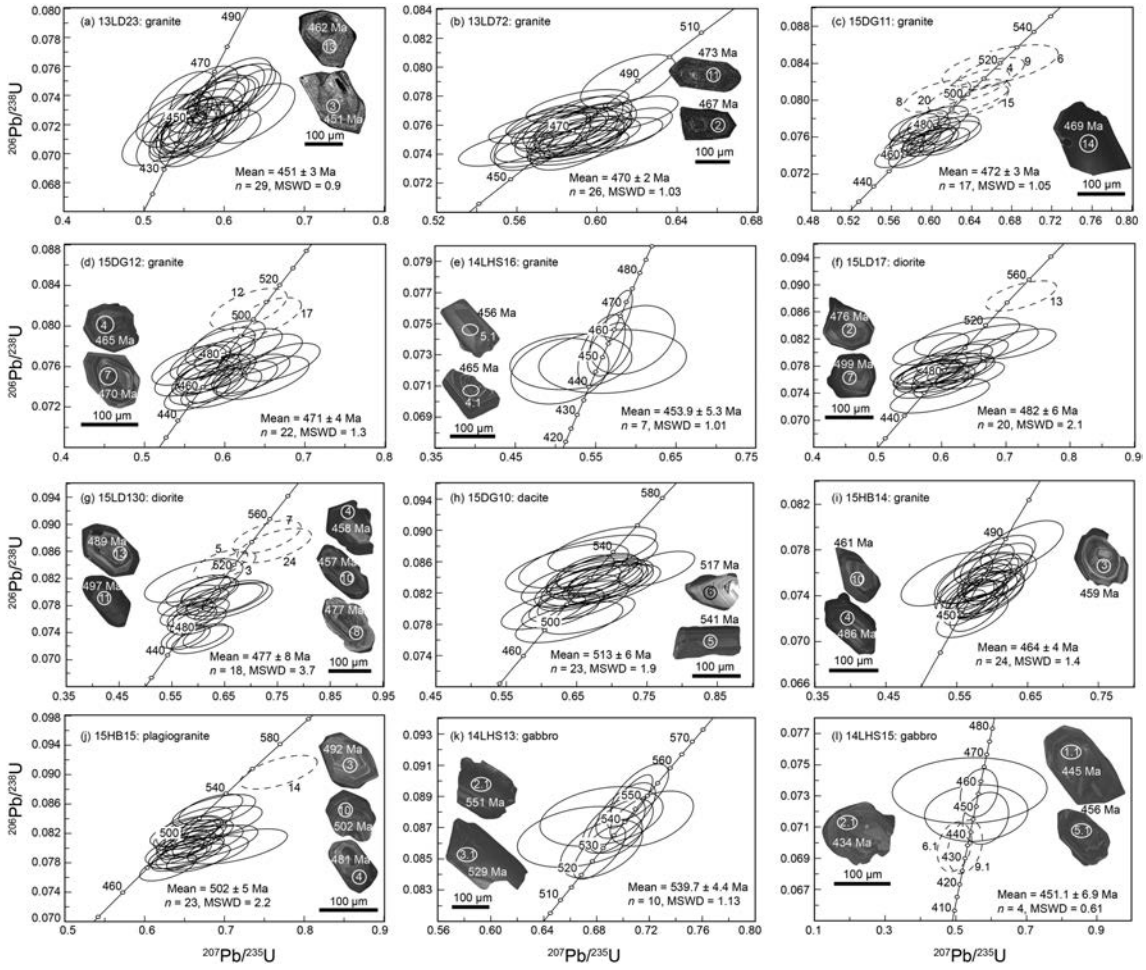

Figure 6. LA-ICP-MS (a–j) and SHRIMP (k–l) zircon U-Pb concordia diagrams for samples igneous clasts. Dotted circles represent discordant ages that were not used to calculate the average weighted age.

decreases. Quartzite clasts are the most variable and abundant lithology within the clast population. Their abundance in the Yaoshuiquan formation (17–59%) is higher than in the Huabaoshan formation (16–24%). Granitoid and andesite clasts are the most abundant igneous populations in both formations. Granitoid clasts have a higher and more variable abundance (9–36%) than andesite (6–23%) and dacite (4–28%) clasts. The total abundance of granitoid, andesite, and dacite clasts in the Yaoshuiquan and Huabaoshan formations is 24–70% and 46–58%, respectively. These igneous clasts decrease in abundance toward the east. The abundance of gabbro, basalt, and chert clasts is generally less than 10%, and serpentinite and limestone clasts mainly occur around the Yuanshishan arc-ophiolite and accretionary complex outcrops. These results suggest a complicated pattern of derivation from different sources.

4.2. U-Pb Ages of Clasts

Fourteen representative clasts including twelve igneous and two quartzite clasts were sampled (Figures 3 and 5) in order to separate zircon grains and then determine U-Pb ages using SHRIMP and LA-ICP-MS methods at Beijing SHRIMP Center, Institute of Geology, Chinese Academy of Geological Sciences, and Beijing Createch Testing Technology Co., Ltd., respectively. Analytical results and methodology for the zircon studies are available in the auxiliary material (Data Set S1, S2, and S3). All analyzed zircon grains are short or long prismatic grains showing well-developed concentric oscillatory and banded zoning in CL images. With the exception of zircon grains analyzed from gabbro clast 14LHS13 with a variable and relative low Th/U ratio of 0.14–0.28, analyzed zircons show banded and concentric oscillatory zoning in CL images and generally have high and variable Th/U ratios (>0.28).

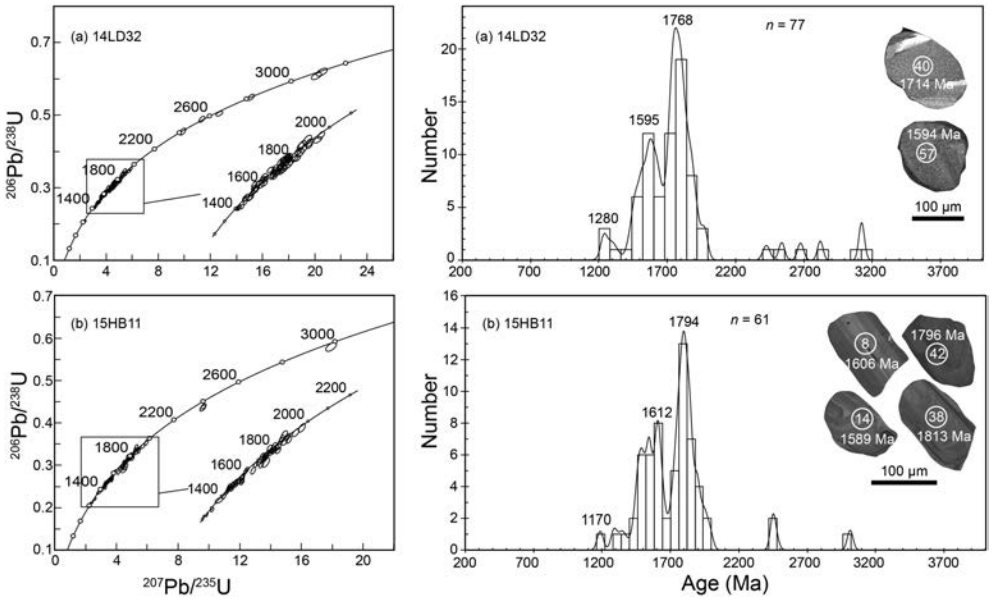

Figure 7. LA-ICP-MS detrital zircon U-Pb concordia diagrams and age spectra and relative age probabilities for quartzite pebbles in the Yaoshuiquan (a) and Huabaoshan (b) formations. Ages and uncertainties were calculated using concordant data (Ludwig, 2003). Zircons older than ca. 1.0 Ga were dated using the $^{207}Pb/^{206}Pb$ age. *n* indicates the number of concordant spots relative to total analyzed spots.

4.2.1. Igneous Clasts

Five granite clasts 13LD23, 13LD72, 15DG11, 15DG12, and 14LHS16 from the Yaoshuiquan Formation yielded weighted mean $^{206}Pb/^{238}U$ ages of 451 ± 3 Ma (MSWD = 0.9), 470 ± 2 Ma (MSWD = 1.03), 472 ± 3 Ma (MSWD = 1.05), 471 ± 4 Ma (MSWD = 1.3), and 453.9 ± 5.3 Ma (MSWD = 1.01), respectively, whereas two diorite clasts 15LD17 and 15LD130 yielded slightly older ages of 482 ± 6 Ma (MSWD = 2.1) and 477 ± 8 Ma (MSWD = 3.7) (Figure 6). Two gabbro clasts 14LHS13 and 14LHS15 yielded weighted mean $^{206}Pb/^{238}U$ ages of 539.7 ± 4.4 Ma (MSWD = 1.13) and 451.1 ± 6.9 Ma (MSWD = 0.61), respectively. Dacite clast 15DG10 yielded a weighted mean $^{206}Pb/^{238}U$ age of 513 ± 5 Ma (MSWD = 2.2). Granite clast 15HB14 and plagiogranite clast 15HB15 from the Huabaoshan formation yielded weighted mean $^{206}Pb/^{238}U$ ages of 464 ± 4 Ma (MSWD = 1.4) and 502 ± 5 Ma (MSWD = 2.2), respectively.

4.2.2. Quartzite Clasts

Detrital zircon grains from two quartzite clasts 14LD32 and 15HB11 collected from the two measured sections through the Yaoshuiquan and Huabaoshan formations yielded similar age spectra (Figure 7) with a main age peak at 1768 Ma and 1794 Ma and a secondary peak at 1599 Ma and 1612 Ma, respectively. Both samples also yielded two minor U-Pb age peaks at ca. 2500 Ma and 3200 Ma, respectively. In addition, sample 15HB11 yielded the youngest age peak at 1170 Ma, which is slightly younger than sample 14LD32 with a minimum age peak at 1280 Ma.

4.3. Sandstone Composition

Sandstones are poorly to moderately sorted, medium- to coarse-grained, and usually exhibit slight alteration of framework grains (Figure 8). In order to define the source area of these sandstones, 97 unweathered sandstones were preferentially sampled to facilitate determination of lithic modes from 8 measured sections, representing the complete range of alluvial fine-grained deposits in the Yaoshuiquan and Huabaoshan formations. A minimum of 300 framework grains were counted and assigned to 14 categories in each sample, using a minimum grain size of 0.063 mm in order to optimize reliability of identification of predominant fine-grained lithic clasts. To compensate for compositional differences between varying grain sizes, grain assignments during point counting followed the Gazzi-Dickinson method (Ingersoll, 1990), such that sand-sized crystals within lithic clasts were counted as separate grains rather than as the host lithic clasts. Criteria used for distinguishing lithic types, matrix types, and other components followed those of

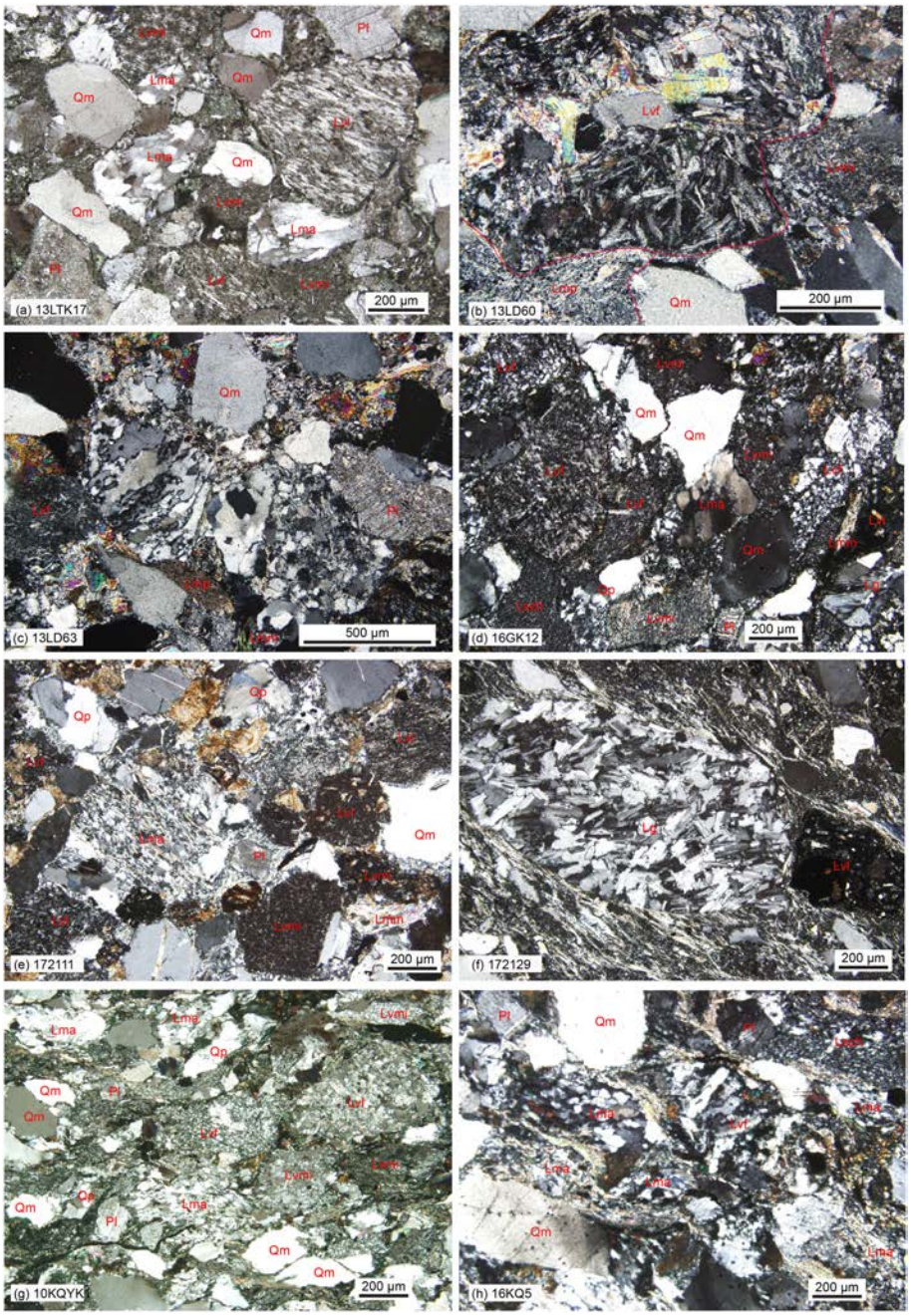

Figure 8. Photomicrographs (cross-polarized light) of grain types inferred to be an important source-rock indicator in sandstones of the Lianhuashan-Huabaoshan foreland basin. (a) to (d) and (e) to (d) are sandstone samples from the Yaoshuiquan and Huabaoshan formations, respectively. Qm = monocrystalline quartz grain; Qp = polycrystalline quartz grain; P = plagioclase grain; Lvf = volcanic lithic fragment with felsic and/or micrographic and/or vermicular quartz clasts; Lvl = volcanic lithic fragments with lathwork texture; Lvmi = volcanic lithic fragments with microlite texture; Lma = feldspar-quartz-mica lithic fragment; Lmp = phyllite lithic fragment; Lmm = polycrystalline mica lithic fragment; Lsch = sedimentary chert and/or cherty argillite lithic fragment; Lg = granite lithic fragment.

Dickinson (1970) and Graham et al. (1976). Raw modal point-count data and recalculated parameters are available in the auxiliary material (Data Set S4 and S5).

On the base of petrographic analysis, common framework grains of the sandstones include angular-subangular lithic, feldspar, and quartz grains and little matrix (<5%). These sandstones are thus subdivided into two distinctive litharenite and feldspathic litharenite petrofacies. Framework grain point-count data

demonstrate a dominance of igneous and metamorphic relative to sedimentary source rocks due to the greater abundance of feldspar and polycrystalline quartz grains, but the relative abundance of monocrystalline quartz and feldspar grains is lower than that of lithic fragments. Subtypes of igneous fragments can be discriminated based on their groundmass textures. They include basalt, andesite, dacite, and granitoids. Metamorphic grains include mica-quartz schist, granitic gneiss, and quartzite. Granitoid grains consist of quartz and plagioclase grains with a clear hypidiomorphic, granular texture, but granitic gneiss grains consist of foliated quartz, feldspar, and minor mica. Mica-quartz schist grains include foliated muscovite and quartz, and quartzites mainly consist of foliated quartz grains. Sedimentary clasts include chert and sandstone but are less abundant than igneous and metamorphic grains.

The abundance of igneous fragments is variable and dramatically decreases eastward from 85% to 11%. The ratio of igneous to total lithic fragments in sandstones of the Huabaoshan formation around the Ayishan area is variable but greater (0.39–0.86) than other sections (0.08–0.55). The relative abundance of metamorphic clasts in the Huabaoshan formation is greater (37–86%) than in the Yaoshuiquan formation (22–72%). Basaltic fragments in sandstones from the Yaoshuiquan and Huabaoshan formations near the Cambrian arc-ophiolite complex are more abundant than they are in sandstones around the Ayishan arc where felsic, andesitic, and metamorphic fragments are common.

Feldspar grains are dominated by detrital plagioclase, showing a variable (0.8–26.5%) and low abundance (average 9.6%) of framework grains. Minor detrital potassium feldspar grains occur in several samples of the Yaoshuiquan formation from the Shihuiyao area. Quartz grains range from 18.6% to 54.8% (average 35.6%) of the framework grains in the Yaoshuiquan and Huabaoshan formations, which is less than lithic grains but greater than feldspar grains. The ratio of polycrystalline quartz to total quartz is variable (0.04–0.37) and relatively low (average 0.18). Most monocrystalline grains are clear and inclusion-free, have uniform extinction, and contain embayed crystal margins, suggestive of a volcanic origin. Polycrystalline quartz grains exhibit undulatory extinction and contain common fluid inclusions that appear to be plutonic (Basu et al., 1975). Some of the polycrystalline quartz grains are longate with a preferred orientation, suggesting derivation from metamorphic rocks.

4.4. Detrital Heavy Mineral Assemblages

For detrital heavy mineral analysis, the sandy matrix of one conglomerate sample and eight sandstone samples from six measured sections (each sample was about 1 kg) were collected. All sample material was first crushed to <2 mm fragments. To ensure that separated heavy minerals were depositional framework grains rather than lithic fragments, a 0.20–0.45 mm grain size fraction for separation of heavy minerals was chosen by gravity setting and using an electromagnetic field. Heavy mineral types were further identified and separated under a binocular microscope. The relative concentration of dense minerals was evaluated followed standard procedures (Mange & Maurer, 1992).

The analytical results demonstrate that detrital zircon, pyrite, and hematite grains are common in sandstones of the Yaoshuiquan and Huabaoshan formations, but the occurrence of detrital magnetite, tourmaline, epidote, garnet, chromite, hornblende, pyroxene, and rutile varies considerably. These grains mostly display irregular, subangular, and subrounded to rounded shapes with distinct erosional pits, suggesting they have experienced long-distance transportation in the processes of deposition.

To best display and emphasize the relative abundance of heavy minerals that are useful in the characterization of source areas, common minerals such as zircon, pyrite, and hematite are not shown on pie charts (Figures 3 and 5). The conglomerate sandy matrix has a similar heavy mineral assemblage to that of the sandstones, including epidote, magnetite, chromite, garnet, and pyroxene. Except for epidote, chromite, and magnetite, sandstones in the Yaoshuiquan formation contain more abundant pyroxene, hornblende, and garnet grains than that of the Huabaoshan formation. Mafic mineral grains decrease in abundance up-section; the proportion of detrital garnet grains increases in both formations, but the inversely variable abundance of these grains also follows a similar trend from south to north.

4.5. Detrital Zircon U-Pb Ages

Nine medium-grain sandstone samples were collected for zircon separation and U-Pb dating together with the sandy matrix of one conglomerate sample 15LD1. Zircon separation and LA-ICP-MS U-Pb dating methods are reported in the auxiliary material (Data Set S1) together with analytical results (Data Set S6).

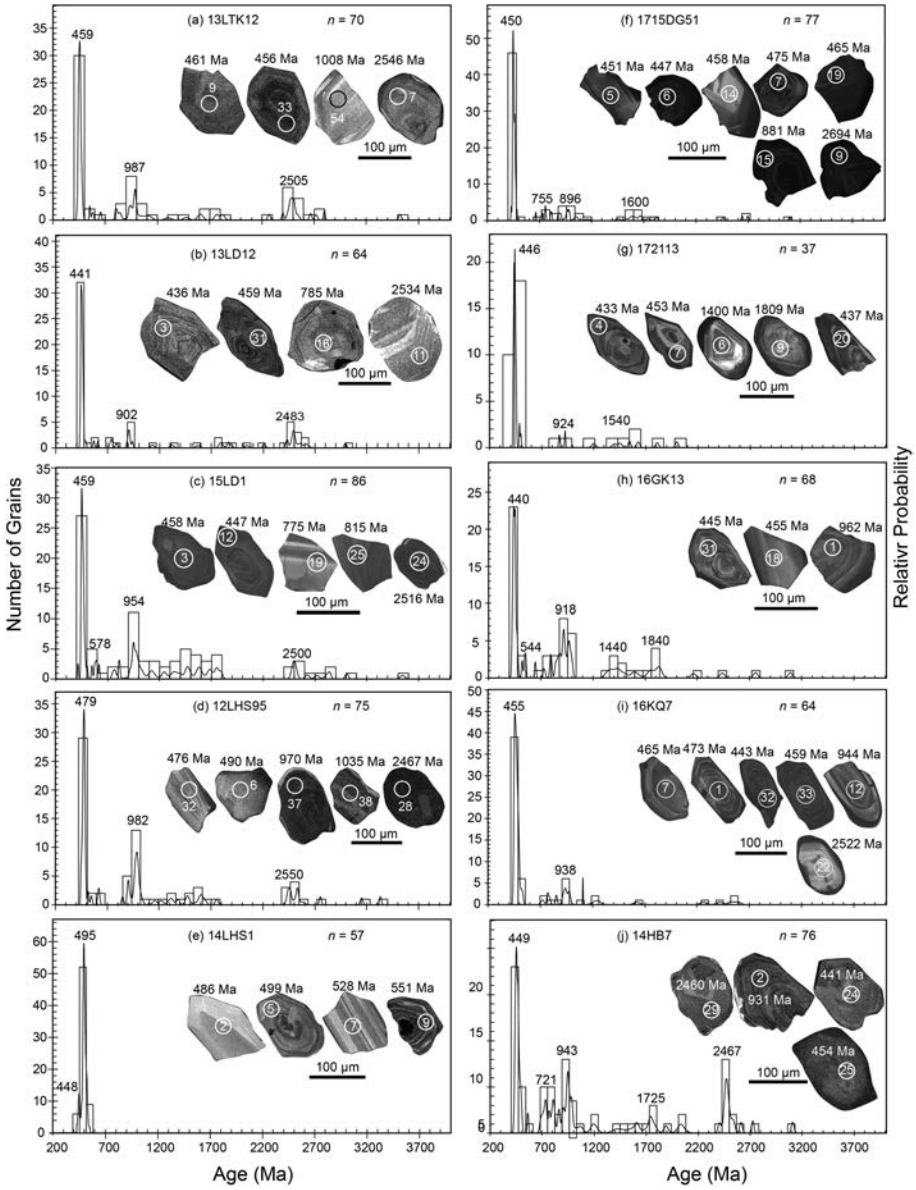

Figure 9. Histograms and relative probability of ages within ±10% of concordia for sandstone samples. (a) to (e) and (f) to (j) were collected from the Yaoshuiquan and Huabaoshan formations, respectively. All U-Pb isotopic data for detrital zircons are LA-ICP-MS data. Ages and uncertainties were calculated using concordant data (Ludwig, 2003). Zircons older than ca. 1.0 Ga were dated using the $^{207}Pb/^{206}Pb$ age, whereas younger zircons used the $^{206}Pb/^{238}U$ age.

4.5.1. Yaoshuiquan Formation

13LTK12 Seventy out of 82 spot analyses yielded concordant $^{206}Pb/^{238}U$ ages ranging from 443 to 3523 Ma with a variable U content of 48–710 ppm and Th/U ratio of 0.04–1.56 (average 0.67). Thirty of the spots yielded Early Paleozoic ages between 443 and 483 Ma with a weighted mean age of 457.0 ± 3.7 Ma (MSWD = 2.0), which also defines a dominant peak at 459 Ma (Figure 9a). Sixteen ages were between 555 and 1,008 Ma, 18 ages between 1,031 and 2,500 Ma, and six Archean ages were between 2,508 and 2,799 Ma. The Precambrian ages display secondary peaks at 987 and 2,505 Ma. One Paleoarchean zircon grain yielded a concordant $^{207}Pb/^{206}Pb$ age of 3523 ± 12 Ma.

13LD12 Sixty-four out of 70 dated detrital zircon grains yielded concordant $^{206}Pb/^{238}U$ ages ranging from 436–2,993 Ma, with a dominant peak at 441 Ma and two minor peaks at 902 and 2,483 Ma (Figure 9b).

Thirty-three ages were between 436 and 486 Ma with a weighted mean age of 448.9 ± 2.9 Ma (MSWD = 2.4). These spots have a variety of U contents (3–897 ppm) and Th/U ratios of 0.18–3.09 (average 0.93).

15LD1 Eighty-six out of 90 dated detrital zircon grains are dominated by Early Paleozoic ages between 444 and 504 Ma (n = 28; ca. 30%) with a main peak at 459 Ma (Figure 9c), which is similar to sample 13LTK12. Forty-seven ages were between 551 and 1798 Ma, and 11 ages between 2483 and 3544 Ma with 2 smaller peaks at 954 and 2500 Ma were also recorded. All analyzed spots have a wide range of U contents (129–2861 ppm) and variable but high Th/U ratios of 0.06–2.12 (average 0.61).

12LHS95 Seventy-five dated detrital zircons yielded concordant $^{206}Pb/^{238}U$ ages of 449–3,333 Ma, with a dominant peak at 479 Ma and two subordinate peaks at 982 and 2550 Ma (Figure 9d). This sample also yielded seven Archean grains ranging from 2508 to 3333 Ma. Twenty-nine ages were between 449 and 493 Ma (ca. 39%) with a weighted mean age of 478.7 ± 3.1 Ma (MSWD = 1.5). The analyzed spots have variable U contents of 16-1274 ppm and Th/U ratios between 0.07 and 1.74 (average 0.65).

14LHS1 This sample was collected from the Shihuiyao section where the sedimentary succession overlies as basement of Cambrian ophiolite. Zircon grains are characterized by banded and concentric oscillatory zoning observed with CL imagery. Fifty-seven out of 76 dated detrital zircons yielded concordant $^{206}Pb/^{238}U$ ages ranging from 437 to 551 Ma, with a main peak at 495 Ma (n = 48) and a minor peak at 448 Ma (n = 9) (Figure 9e). No Proterozoic and Archean ages were obtained from this sample, which may relate to the limited number of zircon grains that were dated. The analyzed spots have variable U contents of 9–874 ppm and Th/U ratios between 0.03–1.33 (average 0.65).

1715DG51 Seventy-seven out of 80 dated detrital zircons yielded concordant $^{206}Pb/^{238}U$ ages ranging from 431 to 3,097 Ma, with a wide range of U (41–962 ppm) and Th (13–758 ppm) contents and high and variable Th/U ratios of 0.19-1.6 (average 0.69). Forty-seven ages were between 431 and 486 Ma with a main peak at 450 Ma (Figure 9f) and a weighted mean age of 455.9 ± 2.7 Ma (MSWD = 7.4; n = 45). Fourteen Neoproterozoic ages lie between 666 and 989 Ma with 12 ages between 1042 and 2461 Ma. In addition, three Archean ages are 2,642, 2,694 and 3,097 Ma.

4.5.2. Huabaoshan Formation

172113 This sample from the Ayishan section contains abundant volcanic fragments (Figure 8e). Thirty-seven out of 40 detrital zircons yielded concordant $^{206}Pb/^{238}U$ ages ranging from 427 to 1,998 Ma, with a main peak at 446 Ma and two minor peaks at 924 and 1,540 Ma (Figure 9g). Twenty-six ages were between 427 and 463 Ma with a weighted mean U-Pb age of 442.8 ± 3.8 Ma (MSWD = 10.7). This sample yielded two Cambrian zircon grains with one grain of 490 Ma and another of 502 Ma. Nine grains yielded Proterozoic ages ranging from 871 to 1,998 Ma. These analyzed spots have variable Th contents of 125–1,022 ppm and Th/U values of 0.1–1.39 (average 0.51).

18GK13 Sixty-eight out of 80 dated detrital zircons yielded a range of concordant $^{206}Pb/^{238}U$ ages from 422 to 3092 Ma, with a main peak at 440 Ma and a subordinate peak at 918 Ma (Figure 9h). In addition, there are three minor peaks at 544, 1,440, and 1,840 Ma. Twenty-three ages were between 422 and 476 Ma (ca. 36%) and one grain was of Cambrian age at 521 ± 6 Ma. Forty ages are Proterozoic ranging from 544 to 2487 Ma, and three Archean grains are present with ages of 2731, 2759, and 3092 Ma. These analyzed spots have variable Th contents of 22–1,214 ppm and Th/U values of 0.03–1.66 (average 0.56). The main peak for this sample is same as that of sample 13LD12 from the Yaoshuiquan formation.

16KQ7 Sixty-four out of the 80 dated detrital zircons yielded a range of concordant $^{206}Pb/^{238}U$ ages from 443 to 2,589 Ma, with a main peak at 455 Ma and a minor peak at 938 Ma (Figure 9i). Forty-five ages ranging from 443 to 530 Ma yielded a weighted mean U-Pb age of 465.7 ± 4.6 Ma (n = 43; MSWD = 6.3). Ten Neoproterozoic ages are from 719 to 977 Ma and six Meso- to Paleo-proterozoic ages between 1106 and 2414 Ma. Two Archean grains are present with ages of 2,522 Ma and 2,589 Ma. All analyzed spots have a variety of Th (19–782 ppm) and U (43–1121) contents, with variable and high Th/U ratios of 0.11–1.32 (average 0.59). The main peak of this sample is similar to that for samples 13LTK12 and 15LD1 from the Yaoshuiquan formation.

14HB7 Seventy-six out of 80 spot analyses from this sample yielded a range of concordant $^{206}Pb/^{238}U$ ages from 435 to 3,110 Ma. Twenty-four ages were between 435 and 494 Ma with a main peak at 449 Ma

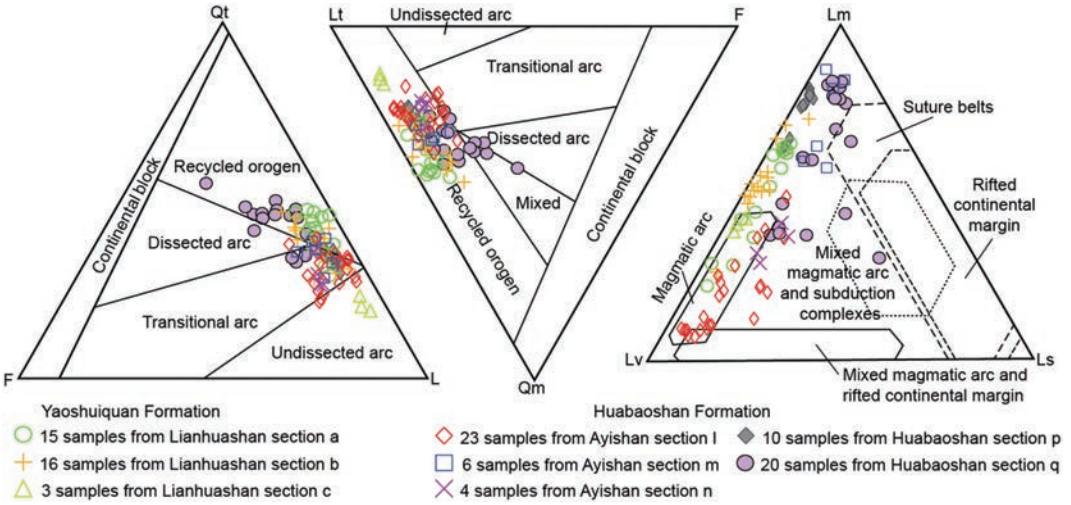

Figure 10. Qt-F-L (left), Qm-F-Lt (middle) and Lm-Lv-Ls (right) diagrams showing spatial evolutionary changes in sandstone compositions from the Yaoshuiquan and Huabaoshan formations (after Dickinson et al., 1983; Ingersoll & Suczek, 1979). Qt, Qm, F, L, and Lt represents total quartz, monocrystalline quartz, total feldspars, lithoclasts, and total lithoclasts including polycrystalline quartz grain, respectively. Lm, Lv, and Ls represent metamorphic, volcanic, and sedimentary clasts, respectively. Note that the dots with different shapes in these diagrams represent an average value of total studied samples in different log, respectively.

(Figure 9j) and twenty-four ages between 560 and 983 Ma with a subordinate peak at 943 Ma. Twenty-four ages range from 1011 to 2,485 Ma with a subordinate peak at 2,467 Ma. In addition, this sample also has five Archean zircons with ages of 2,514, 2,542, 2,613, 2,726, and 3,110 Ma. These analyzed spots have a wide range of U contents (48–1,308 ppm) and high and variable Th/U ratios of 0.13–2.66 (average 0.75). The main peak of 449 Ma is same as that for sample 1715DG51 from the Yaoshuiquan formation, but there are more Paleoproterozoic grains.

5. Paleocurrent Data

A total of 838 planar and trough cross-bedding and imbricated clast orientations were recorded at suitable outcrops in order to provide information on source location and basin paleogeography for the Yaoshuiquan and Huabaoshan formations (Figures 3 and 5). Paleocurrent data were corrected for local dip but not for possible later rotation because of a lack of any regional rotation data to use as reference.

Results demonstrate that lower parts of the sections through both formations have paleocurrent azimuths between 330° and 40°, but the lower levels of the middle part of the sections have dual-direction paleocurrent azimuths of 80° and 260°. The upper and upper-middle parts of the sections reveal similar paleocurrent azimuths between 130°–230°, which differs from lower parts of the section.

6. Discussion

6.1. Depositional Age

Detrital zircon U-Pb data from the sandy conglomerate-matrix (15LD1) indicate the maximum depositional age of this conglomerate is 444 Ma. The youngest igneous clasts (13LD23 and 14LHS15) suggest a maximum depositional age for the conglomerates of 451 Ma. However, the youngest population of detrital zircons from sandstone samples (13LD12, 16GK13, and 172113) demonstrates that their maximum depositional age is no older than 440 Ma. Regionally, the Huabaoshan and Yaoshuiquan formations are intruded by 420 Ma dacite plutons, but a 443 Ma granite porphyry intrusion crosscuts the conglomerate assemblage in the lower levels of the Yaoshuiquan formation in the west of the Shihuiyao accretionary complex. Together, these observations indicate that the Yaoshuiquan and Huabaoshan formations were deposited between 450 and 420 Ma.

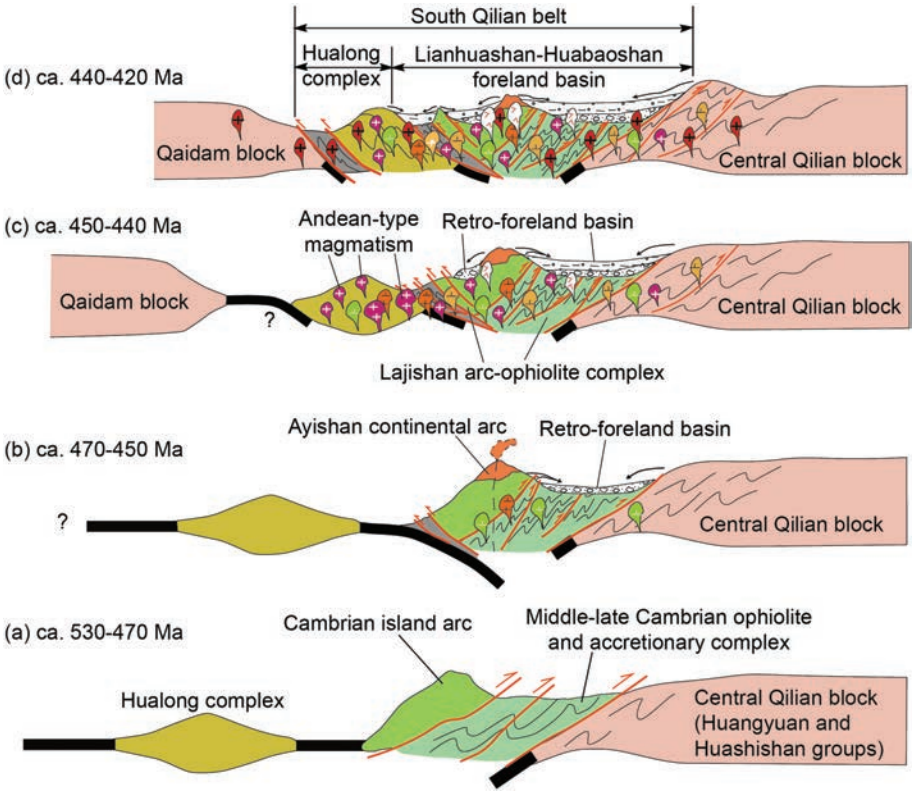

Figure 11. Cartoon diagrams illustrating possible tectonic and depositional relationships for the South Qilian belt during Early Paleozoic time. (a) Circa 530–480 Ma intraoceanic arc-accretionary complex system emplaced onto the Central Qilian block at circa 470 Ma (after Fu et al., 2018). (b) Development of a continental arc and retro-foreland basin following subduction flip between 470–450 Ma. (c) Collision of the Hualong complex against Ayishan arc, formation of a broad Andean-type margin and widening the basin associated with northward subduction of Proto-Tethyan Ocean in front of the Qaidam block from 450 to 440 Ma. (d) Collision of the Qaidam block against the Andean-type margin in response to Proto-Tethyan Ocean closure at circa 440–420 Ma (after Gehrels et al., 2003a, 2003b; Li et al., 2018).

6.2. Provenance

Together, paleocurrent, compositional, geochronological and geological mapping results demonstrate that the Precambrian Huangyuan Group and early Paleozoic arc-ophiolite complex along the current boundaries between the South and Central Qilian belts were the main sources of sediment shed into the Lianhuashan-Huabaoshan basin. Voluminous poorly sorted alluvial conglomerates on the southern side of the basin are dominated by detritus derived from an arc-ophiolite complex. However, coarse- and fine-grained braid channel and floodplain deposits in the center and northern side of the basin contain abundant metamorphic fragments originating from the Huangyuan Group in the Central Qilian block. These variations indicate a northward migration of the depocenter over time from 450 to 420 Ma.

Sandstones adjacent to the arc-ophiolite complex and Ayishan arc plot within the ‘transitional arc’ and ‘undissected arc’ detrital provenance fields on the Qt-F-L plot of Dickinson et al. (1983), whereas on a Qm-F-Lt plot all samples plot within the ‘recycled orogen’ field (Figure 10). In order to clearly differentiate potential source rocks, lithic populations were examined and then plotted using the Lm-Lv-Ls plot of Ingersoll and Suczek (1979). Sandstone samples proximal to the Ayishan arc all plotted within the ‘magmatic arc’ field, but other samples plotted outside of this field and in and around the ‘suture belt’ field. This suggests that metasedimentary and high-grade gneiss terranes existed in the source area (Ingersoll & Suczek, 1979) and their erosion contributed voluminous metamorphic detritus. In particular, samples from Huabaoshan sections plot both within the ‘recycled orogen’ and overlap with the ‘suture belt’ fields in Qt-F-L and Lm-Lv-Ls plots, respectively, indicating a source area dominated by metamorphic rocks. In light of generally both northward and southward paleocurrent indicators, these results suggest sediment

derivation from rocks both the Huangyuan Group and the 'suture belt' on the southern side of the arc-ophiolite complex.

Zircon U-Pb age data from sandstones and igneous clasts further demonstrate a mixed source. Together with chert, basalt, limestone, and serpentinite clasts and 495 Ma detrital zircon populations as well as 540 Ma gabbro, 513 Ma dacite, and 502 Ma plagiogranite clasts were most likely derived from the Cambrian-age arc-ophiolite complex on the south side of the basin. Ordovician detrital zircon populations (ca. 480–440 Ma) that correspond with the ages of granitoid clasts were almost certainly derived from the Ayishan arc, whereas coeval I- and S-type granitoid intrusions in the Central Qilian block and Hualong complex (Tung et al., 2016; Yan et al., 2015) also contributed voluminous ca. 450–440 Ma detrital zircon populations. Neoproterozoic (ca. 987–721 Ma) quartzite pebbles and detrital zircon populations indicate a Huangyuan Group source, but minor Archean and Meso- and Paleoproterozoic detrital zircon populations in sandstones and quartzite pebbles overlap with the ages of high-grade metasedimentary rocks of the Central Qilian Block (Gehrels et al., 2003a; Lu et al., 2009).

6.3. Tectonic Implications

The Yaoshuiquan and Huabaoshan formations were deposited in a similar sedimentary environment and have similar rock associations, comprising massive conglomerate, lenticular coarse-grained sandstone and conglomerate, and thick siltstone and mudstone. They both show an upward and northward fining sequence with typical alluvial deposits. Abundant arc-ophiolite fragments and the associated mineral grains of chromite, pyroxene, magnetite, and epidote mainly occur in the lower sequence, and their abundance decreases quickly up-section. The abundance of metamorphic clasts (quartzite, schist, and gneiss) and associated garnet grains also increases voluminously upward. In addition, both formations show NNW to NNE of paleocurrent direction in the lower part of their sections, near N-W directions in the lower middle, and then SE to SW directions at higher level of the middle and upper parts of the sections. These results indicate source and overall basin evolution patterns similar to those described from the Cretaceous Neuquén Basin in the western South America (Di Giulio et al., 2017), Silurian sedimentary basin in the Lachlan Fold Belt (Aitchison & Buckman, 2012), and western foreland basin in Taiwan (Huang et al., 2006; Lundberg & Dorsey, 1988). Regional radial- and along-strike lithofacies and compositional trends and associated paleocurrent indicators of both formations are consistent with a model for primarily south to north-direction radial and east to west-direction axial sediment transport in an arc-continent collision-related retro-foreland basin (Jordan, 1995). The alluvial sediments we investigated record the influx, into this retro-foreland basin, of clastic sediments derived mainly from an arc-ophiolite complex provenance initially. There was a progressive shift to a mixed continental basement provenance as the arc-continent collision progressed and deeper crustal levels were uplifted, exposed and eroded. Development of the basin likely also heralded the initial closure of the Proto-Tethyan Ocean associated with this part of the NE Tibet Plateau.

Together with our new mapping, petrologic, mineral, and geochemical data, the Lajishan arc-ophiolite complex represents a Cambrian intraoceanic subduction system that formed in response to southward subduction of the Proto-Tethyan Ocean from circa 530–470 Ma (Figure 11a; Fu & Yan, 2017; Fu et al., 2018; Yan et al., 2019). As this complex collided with the Central Qilian block subduction polarity flipped in a manner similar to that observed in the presently active arc-continent collision system of Taiwan. A north-facing subduction system and associated Andean-type arc began to develop along the southern of the central Qilian block between 470–450 Ma (Gehrels et al., 2003a; Tung et al., 2016; Yan et al., 2019). Voluminous dacite, rhyolite, and the associated volcaniclastic rocks in the Ayishan area nonconformably overlie the Cambrian arc-ophiolite and accretionary complexes. The corresponding rocks in the west of the northern South Qilian belt include andesite, dacite, and rhyolites that exhibit typical subduction-related calc-alkaline geochemical affinity (Niu et al., 2016; Yan et al., 2019). Synchronous subduction-related I-type (Fu & Yan, 2017; Wu et al., 2009; Yu et al., 2018) granitoids intruded into the Cambrian arc-ophiolite complex and accretionary complex in the South Qilian belt. Igneous arc activity took place in the Central Qilian belt from ca. 520–440 Ma (Gehrels et al., 2003; Yong et al., 2008; Song et al., 2013; Tung et al., 2016; Wu et al., 2016). The trend of magmatic termination ages becomes younger in a southward direction (Wu et al., 2016) as result of northward subduction of the Proto-Tethyan Ocean. A corresponding retro-foreland basin (Figure 11b), which lay behind this arc, also formed and began to receive voluminous coarse-grained detritus from the arc and older arc-ophiolite complex.

Between 450 to 440 Ma, the Hualong complex was accreted to the north and amalgamated with the Central Qilian block. Northward subduction of the Proto-Tethyan Ocean occurred along the southern margin of the Hualong complex. Thus, voluminous 450–440 Ma arc-related I-type granites (Tung et al., 2016; Yan et al., 2015) that straddle the Central and South Qilian belts formed a broad Andean-type continental margin (Yan et al., 2019). Voluminous detritus shed from the Central Qilian Block and the uplifted Cambrian-age arc-ophiolite complex accumulated in the basin (Figure 11c) to which the Ordovician-age Ayishan arc also contributed abundant detritus.

Between around 440 to 420 Ma, the Proto-Tethyan Ocean closed and the Qaidam block collided against this Andean-type margin (Figure 11d). This event is represented by voluminous 440–420 Ma syncollisional and postcollisional granitoids, associated high-pressure granulite-facies metamorphism in the South Qilian belt and the Qaidam block and accompanying anatexis (Li et al., 2018; Yan et al., 2015; Yu et al., 2014; Zhang et al., 2015). The collision resulted in uplift and erosion of the Hualong complex and the Central Qilian block, which contributed additional metamorphic detritus into the basin. In addition, a dextral strike-slip shear zone also developed in the Central Qilian block during this collision event (Qi et al., 2004).

7. Conclusions

(1) The Yaoshuiquan and Huabaoshan formations in the South Qilian belt are northward-fining alluvial deposits of a retro-foreland basin that formed in response to arc-continent collision in the NE Tibetan Plateau during 470–420 Ma.

(2) A broad Andean-type continental margin formed on the NE Tibetan Plateau in response to northward-subduction of the Proto-Tethyan Ocean from 470 to 440 Ma.

(3) Collision of the Qaidam block against this Andean-type margin corresponds to the closure of the Proto-Tethyan Ocean around 440–420 Ma.

(4) Deposition within the Lianhuashan-Huabaoshan retro-foreland basin was with primarily south to north-directed radial and east to west-directed axial sediment transport.

Acknowledgments
The study was funded by the National Natural Science Foundation of China (41872241, 41672221, and 41702239) and China Geological Survey (DD20160201-04 and DD20160022-02). We are grateful to Editor John Geissman, Associate Editor Andrei Khudoley, reviewer Dr. Chen Wu, and an anonymous reviewer whose critical comments and constructive evaluation have significantly improved the quality of the paper. The data used are available in the supporting information, which can be downloaded from the University of Queensland eSpace data repository website (https://doi.org/10.14264/uql.2019.684).

References

Aitchison, J. C., Badengzhu, A., Davis, M., Liu, J., Luo, H., Malpas, J. G., et al. (2000). Remnants of a Cretaceous intra-oceanic subduction system within the Yarlung-Zangbo suture (southern Tibet). *Earth and Planetary Science Letters*, *183*(1-2), 231–244.

Aitchison, J. C., & Buckman, S. (2012). Accordion vs. quantum tectonics: Insights into continental growth processes from the Paleozoic of eastern Gondwana. *Gondwana Research*, *22*(2), 674–680.

Basu, A., Young, S. W., Suttner, L. J., James, W. C., & Mack, G. H. (1975). Reevaluation of the use of undulatory extinction and polycrystallinity in detrital quartz for provenance interpretation. *Journal of Sedimentary Petrology*, *45*, 873–882.

BGMRQP (Bureau of Geology and Mineral Resources of Qinghai Province), (1964). Geological report of Xining (J-47-36) and Ledu (J-48-31) areas [in Chinese], scale 1:200000.

BGMRQP (Bureau of Geology and Mineral Resources of Qinghai Province), (1976). Geological report of Angsiduo (J-48-133-A), Zhabazhen (J-47-144-B), Xiahuancang (J-47-XXII), and Gangchadadi (J-47-XXIII) areas [in Chinese], scale 1:50000.

BGMRQP (Bureau of Geology and Mineral Resources of Qinghai Province), (1991). Regional geology of Qinghai Province [in Chinese], pp. 1-662, Geological Publishing House, Beijing.

Brown, D., & Ryan, P. D. (2011). *Arc-Continent Collision* (p. 725). Frontiers in Earth Sciences: Springer.

Buckman, S., Aitchison, J. C., Nutman, A. P., Bennett, V. C., Saktura, W. M., Walsh, J. M. J., et al. (2018). The Spongtang Massif in Ladakh, NW Himalaya: An Early Cretaceous record of spontaneous, intra-oceanic subduction initiation in the Neotethys. *Gondwana Research*, *63*, 226–249.

Chen, W. S., Eidgway, K. D., Hong, C. S., Chen, Y. G., Shen, K., & Yeh, M. G. (2001). Stratigraphic architecture, magnetostratigraphy, and incised-valley systems of the Pliocene-Pleistocene collisional marine foreland basin of Taiwan. *Geological Society of America Bulletin*, *113*, 1249–1271.

Clift, P. D., Carter, A., Draut, A. E., Long, H. V., Chew, D. M., & Schouten, H. A. (2009). Detrital U-Pb zircon dating of lower Ordovician syn-arc-continent collision conglomerates in the Irish Caledonides. *Tectonophysics*, *479*(1-2), 165–174.

Clift, P. D., Schouten, H., & Draut, A. E. (2003). A general model of arc-continent collision and subduction polarity reversal from Taiwan and the Irish Caledonides. *Geological Society London Special Publication*, *219*, 81–98.

Cooper, P., & Taylor, B. (1987). Seismotectonics of New Guinea: A model for arc reversal following arc-continent collision. *Tectonics*, *6*, 53–67.

Corfield, R. I., & Searle, M. P. (2000). Crustal shortening estimates across the north Indian continental margin, Ladakh, NW India. *Geological Society London Special Publications*, *170*, 395–410.

Dewey, J. F. (2005). Orogeny can be very short. *Proceedings of the National Academy of Sciences*, *102*, 15,286–15,293.

Di Giulio, A., Ronchi, A., Sanfilippo, A., Balgord, E. A., Carrapa, B., & Ramos, V. A. (2017). Cretaceous evolution of the Andean margin between 36° S and 40° S latitude through a multi-proxy provenance analysis of Neuquén Basin strata (Argentina). *Basin Research*, *29*(3), 284–304.

Dickinson, W. R. (1970). Interpreting detrital modes of graywacke and arkose. *Journal of Sedimentary Petrology*, *40*, 695–707.

Dickinson, W. R., Beach, L. S., Brackenridge, G. R., Lindberg, F. A., & Ryberg, P. T. (1983). Provenance of North American Phanerozoic sandstones in relation to tectonic setting. *Geological Society of America Bulletin*, *94*, 222–235.
Dürr, S. B. (1994). Quick estimation of pebble volumes. *Journal of Sedimentary Research*, *64*, 677–679.
Fu, C. L., & Yan, Z. (2017). The composition, age and tectonic setting of Lajishan ophiolitic mélange [in Chinese with English abstract]. *Acta Geoscientica Sinica*, *38*(S1), 29–32.
Fu, C. L., Yan, Z., Guo, X. Q., Niu, M. L., Xia, W. J., Wang, Z. Q., & Li, J. L. (2014). Geochemistry and SHRIMP zircon U-Pb age of diabases in the Lajishankou ophiolitic mélange, South Qilian terrane [in Chinese with English abstract]. *Acta Petrologica Sinica*, *30*(6), 1695–1706.
Fu, C. L., Yan, Z., Wang, Z. Q., Buckman, S., Aitchison, J. C., Niu, M. L., et al. (2018). Lajishankou ophiolite complex: Implications for Paleozoic multiple accretionary and collisional events in the South Qilian belt. *Tectonics*, *37*, 1321–1346. https://doi.org/10.1029/2017TC004740
Galewsky, J., & Silver, I. (1997). Tectonic controls on facies transitions in an oblique collision: The western Solomon Sea, Papua New Guinea. *Geological Society of America Bulletin*, *109*, 1266–1278.
Gehrels, G. E., Yin, A., & Wang, X. (2003a). Magmatic history of the northeastern Tibetan Plateau. *Journal of Geophysical Research*, *108*(B9), 2423. https://doi.org/10.1029/2002JB001876
Gehrels, G. E., Yin, A., & Wang, X. (2003b). Detrital-zircon geochronology of the northeastern Tibetan Plateau. *Geological Society of America Bulletin*, *115*(7), 881–896.
Graham, S. A., Ingersoll, R. V., & Dickinson, W. R. (1976). Common provenance for lithic grains in Carboniferous sandstones from Ouachita Mountains and Black Warrior basin. *Journal of Sedimentary Petrology*, *46*, 620–632.
Guo, J. J., & Li, H. K. (1999). Angular unconformity between the Huashishan Group and Huangzhong Group in the Eastern Mid-Qilian Massif: Identification and implications [in Chinese with English abstract]. *Progress in Precambrian Research*, *22*, 47–52.
Huang, C. Y., Yuan, P. B., & Tsao, S. J. (2006). Temporal and spatial records of active arc-continent collision in Taiwan: A synthesis. *Geological Society of America Bulletin*, *118*, 274–288.
Ingersoll, R. V. (1990). Actualistic sandstone petrofacies: Discriminating modern and ancient source rocks. *Geology*, *18*, 733–736.
Ingersoll, R. V., & Suczek, C. A. (1979). Petrology and provenance of Neogene sand from Nicobar and Bengal Fans, DSDP sites 211 and 218. *Journal of Sedimentary Petrology*, *49*, 1217–1228.
Jordan, T. E. (1995). Retroarc foreland and related basins. In C. J. Busby & R. V. Ingersoll (Eds.), *Tectonics of Sedimentary Basins* (pp. 393–424). Cambridge: Blackwell Science.
Kapp, P., & Decelles, P. (2019). Mesozoic-Cenozoic geological evolution of the Himalayan-Tibetan orogen and working tectonic hypotheses. *American Journal of Science*, *319*, 159–254.
Li, Y., Tong, X., Zhu, Y., Lin, J., Zheng, J., & Brouwer, F. M. (2018). Tectonic affinity and evolution of the Precambrian Qilian block: Insights from petrology, geochemistry and geochronology of the Hualong Group in the Qilian Orogen, NW China. *Precambrian Research*, *315*, 179–200.
Lin, T. R., Peng, S. C., & Zhou, Z. Q. (2015). Cambrian agnostoid trilobites from the Nidanshan and Liudaogou Groups, Hualong, northeastern Qinghai, China [in Chinese with English abstract]. *Acta Palaeontologica Sinica*, *54*(2), 184–206.
Lin, T. R., Peng, S. C., Zhou, Z. Q., & Yang, X. F. (2013). Cambrian polymerid trilobites from the Nidanshan and Liudaogou Groups, Hualong, northeastern Qinghai, China [in Chinese with English abstract]. *Acta Palaeontologica Sinica*, *52*(4), 424–458.
Liu, C., Wu, C., Zhou, Z., Yan, Z., Jiang, T., Song, Z., et al. (2018). U-Pb detrital zircon geochronology from the basement of the Central Qilian Terrane: Implications for tectonic evolution of northeastern Tibetan Plateau. *International Journal of Journal of Earth Science*, *107*, 673–686.
Lu, S. N., Li, H. K., Wang, H. C., Chen, Z. H., Zheng, J. K., & Xiang, Z. Q. (2009). Detrital zircon population of Proterozoic metasedimentary strata in the Qinling-Qilian-Kunlun Orogen [in Chinese with English abstract]. *Acta Petrologica Sinica*, *25*(9), 2195–2208.
Ludwig, K. R. (2003). Isoplot 3.0: A geochronological toolkit for Microsoft Excel. *Berkeley Geochronology Center Special Publication*, *4*, 1–70.
Lundberg, N., & Dorsey, R. J. (1988). Synorogenic sedimentation and subsidence in a Plio-Pleistocene collision basin, eastern Taiwan. In K. Kleinspehn & P. Paloa (Eds.), *New Perspectives in Basin Analysis* (pp. 265–280). New York: Springer-Verlag.
Mange, M. A., & Maurer, H. F. W. (1992). *Heavy minerals in colour* (pp. 1–147). London: Chapman and Hall.
Miall, A. D. (1985). Architectural-element analysis: A new method of facies analysis applied to fluvial deposits. *Earth-Science Reviews*, *22*, 261–308.
Niu, G. Z., Huang, G., Deng, C. S., Xu, Y., Chen, T., Ji, C., & Li, W. J. (2016). LA-ICP-MS zircon U-Pb ages of metamorphic volcanic rocks in Balonggongge'er Formation of South Qilian Mountain in Qinghai Province and their geological significance [in Chinese with English abstract]. *Geological Bulletin of China*, *35*, 1441–1447.
Qi, X.-X., Zhang, J.-X., Li, H.-B., & Cai, J.-L. (2004). Geochronology of the dextral strike ductile shear zone in south margin of the Northern Qilian Mountains and its geological significance. *Earth Science Frontiers*, *11*, 469–479.
Sano, H., & Kanmera, K. (1988). Paleogeographic reconstruction of accreted oceanic rocks, Akiyoshi, southwest Japan. *Geology*, *16*(7), 600–603.
Saqab, M. M., Bourget, J., Trotter, J., & Keep, M. (2017). New constraints on the timing of flexural deformation along the northern Australian margin: Implications for arc-continent collision and the development of the Timor Trough. *Tectonophysics*, *696-697*, 14–36.
Şengör, A. M. C., & Natal'in, B. A. (1996). Paleotectonics of Asia: Fragments of a synthesis. In A. Yin & T. M. Harrison (Eds.), *The Tectonics of Asia* (pp. 486–640). New York: Cambridge University Press.
Smith, A. D., Wen, D. J., Huang, L. Y., & Wang, C. S. (2000). Constraints from gneisses in the Qilian fold belt for the position of the North China block in the Proterozoic [in Chinese with English abstract]. *Journal of the Geological Society of China*, *43*, 81–93.
Sobel, E. R., & Arnaud, N. (1999). A possible middle Paleozoic suture in the Altyn Tagh, NW China. *Tectonics*, *18*(1), 64–74.
Sone, M., & Metcalfe, I. (2008). Parallel Tethyan sutures in mainland Southeast Asia: New insights for Palaeo-Tethys closure and implications for the Indosinian orogeny. *Comptes Rendus Geoscience*, *340*, 166–179.
Song, S., Yang, L., Zhang, Y., Niu, Y., Wang, C., Su, L., & Gao, Y. (2017). Qi-Qin accretionary belt in Central China Orogen: Accretion by trench jam of oceanic Plateau and formation of intra-oceanic arc in the Early Paleozoic Qin-Qi-Kun Ocean. *Science Bulletin*, *62*, 1035–1038.
Song, S. G., Niu, Y. L., Su, L., & Xia, X. H. (2013). Tectonics of the North Qilian Orogen, NW China. *Gondwana Research*, *23*, 1378–1401.
Steel, R. J., & Thompson, D. J. (1983). Structures and textures in Triassic braided stream conglomerates ('Bunter' Pebble Beds) in the Sherwood Sandstone Group, North Staffordshire, England. *Sedimentology*, *30*, 341–367.
Tung, K. A., Yang, H. Y., Liu, D. Y., Zhang, J. X., Yang, H. J., Shau, Y. H., & Tseng, C. Y. (2013). The Neoproterozoic granitoids from the Qilian block, NW China: Evidence for a link between the Qilian and South China blocks. *Precambrian Research*, *235*, 163–189.

Tung, K. A., Yang, H. Y., Yang, H. J., Smith, A., Liu, D., Zhang, J., et al. (2016). Magma sources and petrogenesis of the early-middle Paleozoic backarc granitoids from the central part of the Qilian block, NW China. *Gondwana Research*, *38*, 197–219.

Wan, Y. S., Xu, Z. Q., Yang, J. S., & Zhang, J. X. (2003). The Precambrian high-grade basement of the Qilian terrane and neighboring areas: Its ages and compositions (in Chinese with English abstract). *Acta Geoscientia Sinica*, *24*, 319–324.

Wang, T., Ma, Z., Wang, Z., Zhang, H., & Wang, D. (2016). Constraints of the provenance and deposition time of the early Paleozoic sedimentary rocks in the Lajishan area, Central Qilian [in Chinese with English abstract]. *Acta Geologica Sinica*, *90*(9), 2316–2333.

Wu, C., Wooden, J. L., Robinson, P. T., Gao, Y., Wu, S., Chen, Q., et al. (2009). Geochemistry and zircon SHRIMP U-Pb dating of granitoids from the west segment in the North Qaidam. *Science China (Series D)*, *52*, 1771–1790.

Wu, C., Yin, A., Zhang, J. Y., Liu, W. C., & Ding, L. (2016). Pre-Cenozoic geologic history of the central and northern Tibetan Plateau and the role of Wilson cycles in constructing the Tethyan orogenic system. *Lithosphere*, *8*, 254–292.

Wu, C., Zuza, A. V., Yin, A., Liu, C., Reith, R. C., Zhang, J., et al. (2017). Geochronology and geochemistry of Neoproterozoic granitoids in the central Qilian Shan of northern Tibet: Reconstructing the amalgamation processes and tectonic history of Asia. *Lithosphere*, *9*, L640.1.

Xia, L. Q., Xia, Z. C., & Xu, X. Y. (2003). Magmagenesis in the Ordovician backarc basins of the northern Qilian Mountains, China. *Geological Society of America Bulletin*, *115*, 1510–1522.

Xiao, W. J., Windley, B. F., Yong, Y., Yan, Z., Yuan, C., Liu, C. Z., & Li, J. L. (2009). Early Paleozoic to Devonian multiple-accretionary model for the Qilian Shan, NW China. *Journal of Asian Earth Sciences*, *35*, 323–333.

Xiong, J., & Coney, P. J. (1985). Accreted terranes of China. In D. G. Howell (Ed.), *Tectonostratigraphic Terranes of the Circum-Pacific Region*, *Circum Pacific Council for Energy and Mineral Resources, Earth Science Series No. 1* (pp. 349–361). Houston, TX: The AAPG/Datapages Combined Publications Database.

Yan, Z., Aitchison, J., Fu, C. L., Guo, X. Q., Niu, M. L., Xiao, W. J., & Li, J. L. (2015). Hualong Complex, South Qilian terrane: U-Pb and Lu-Hf constraints on Neoproterozoic micro-continental fragments accreted to the northern Proto-Tethyan margin. *Precambrian Research*, *216*, 65–82.

Yan, Z., Fu, C., Aitchison, J. C., Niu, M., Buckman, S., & Cao, B. (2019). Early Cambrian Muli arc-ophiolite complex: A relic of the Proto-Tethys oceanic lithosphere in the Qilian Orogen, NW China. *International Journal of Earth Sciences*, *108*(4), 1147–1164. https://doi.org/10.1007/s00531-019-01699-6

Yan, Z., Xiao, W. J., Windley, B. F., Wang, Z. Q., & Li, J. L. (2010). Silurian clastic sediments in the North Qilian Shan, NW China: Chemical and isotopic constraints on their forearc provenance with implications for the Paleozoic evolution of the Tibetan Plateau. *Sedimentary Geology*, *231*, 98–114.

Yin, A., & Harrison, T. M. (2000). Geologic evolution of the Himalayan-Tibetan orogeny. *Annual Review of Earth and Planetary Sciences*, *28*, 211–280.

Yin, A., Manning, C. E., Lovera, O., Menold, C. A., Chen, X., & Gehrels, G. E. (2007). Early Paleozoic tectonic and thermomechanical evolution of ultrahigh-pressure (UHP) metamorphic rocks in the northern Tibetan Plateau, northwest China. *International Geology Review*, *49*, 681–716.

Yong, Y., Xiao, W. J., Yuan, C., Yan, Z., & Li, J. L. (2008). Geochronology and geochemistry of Paleozoic granitic plutons from the eastern Central Qilian and their tectonic implications [in Chinese with English abstract]. *Acta Petrologica Sinica*, *24*, 855–866.

Yu, S., Zhang, Z., Mattinson, C. G., del Real, P. G., Li, Y., & Gong, J. (2014). Paleozoic HP granulite-facies metamorphism and anatexis in the Dulan area of the North Qaidam UHP terrane, western China: Constraints from petrology, zircon U-Pb and amphibole Ar-Ar geochronology. *Lithos*, *198-199*, 58–76.

Yu, X.-L., Cai, C.-L., Wei, X.-L., Liu, X.-X., & Yue, X. (2018). Zircon U-Pb geochronology, geochemical characteristics and geological significance of Middle Ordovician intrusive rocks in Shulennanshan area of South Qilian [in Chinese with English abstract]. *Mineral Exploration*, *9*, 2049–2058.

Zhang, J. X., Yu, S. Y., Li, Y. S., Yu, X. X., Lin, Y. H., & Mao, X. H. (2015). Subduction, accretion and closure of Proto-Tethyan Ocean: Early Paleozoic accretion/collision orogeny in the Altun-Qilian-North Qaidam orogenic system [in Chinese with English abstract]. *Acta Petrologica Sinica*, *31*(12), 3531–3554.

Zhang, Q., Buckman, S., Bennett, V. C., & Nutman, A. (2019). Inception and early evolution of the Ordovician Macquarie arc of eastern Gondwana margin: Zircon U-Pb-Hf evidence from the Molong volcanic belt. *Lachlan orogen, Lithos*, *326-327*, 513–528.

Zuo, G., Li, Z., & Zhang, C. (2001). Lajishan tectonic zone of Qinghai province: Rift or tectonic window? [in Chinese with English abstract]. *Geological Review*, *47*(6), 561–566.

Zuza, A. V., Wu, C., Reith, R. C., Yin, A., Li, J., Zhang, J., et al. (2018). Tectonic evolution of the Qilian Shan: An early Paleozoic orogen reactivated in the Cenozoic. *Geological Society of America Bulletin*, *130*(5/6), 881–925.